Coordination Chemistry Reviews 255 (2011) 1587–1602

Contents lists available at ScienceDirect

Coordination Chemistry Reviews

journal homepage: www.elsevier.com/locate/ccr

Review

Functionalization of flat Si surfaces with inorganic compounds—Towards molecular CMOS hybrid devices

Steven P. Cummings, Julia Savchenko, Tong Ren*

Department of Chemistry, Purdue University, West Lafayette, IN 47907, USA

Contents

ARTICLE INFO

Article history:
Received 25 October 2010
Accepted 22 December 2010
Available online 11 January 2011

Keywords:
Molecular passivation
Si surfaces
Inorganic modifiers
Interfacial charge transfer
Molecular devices

ABSTRACT

Covalent modification of flat silicon surfaces is a key step in integrating CMOS technology and molecular electronics that may lead to novel hybrid microelectronic devices. While much of the research has been focused on the functionalization of Si by organic compounds, interest in the functionalization with metal-containing species has intensified in recent years because of the unique attributes of inorganic species including rich redox characteristics and high ground state spins. Described in this short review are (i) synthetic approaches to immobilize inorganic compounds; (ii) structural, spectroscopic and voltammetric techniques for characterization of molecular layers; and (iii) preliminary device fabrication.

1. Introduction

The continuous geometrical scaling of Si-based CMOS (complementary metal–oxide–semiconductor) transistors faces a multitude of technical hurdles that challenges materials sciences and engineering, such as the lack of effective dielectric materials at nanometer scale and an ever increasing power density. Hybrid transistors that incorporate organic/inorganic molecules into embedded interfaces of CMOS devices have been speculated as a promising alternative [1].

Abbreviations: ALD, atomic layer deposition; CEG, cathodic electrografting; CVD, chemical vapor deposition; CV, cyclic voltammetry; I_D, drain current; IPES, inverse photoemission spectroscopy; k_0, rate of electron transfer; MOSFET, metal–oxide–semiconductor field effect transistor; NHE, normal hydrogen electrode; OCP, open circuit potential; SAM, self assembled monolayer; STM, scanning tunneling microscopy; UHV, ultra high vacuum; UPS, ultraviolet photoelectron spectroscopy; υ, scan rate ($V\,s^{-1}$); V_T, threshold voltage; WCA, water contact angle; XPS, X-ray photoelectron spectroscopy.

* Corresponding author.
E-mail address: tren@purdue.edu (T. Ren).

0010-8545/$ – see front matter © 2011 Elsevier B.V. All rights reserved.
doi:10.1016/j.ccr.2010.12.030

An essential starting point for such hybrid devices is the covalent attachment of molecules to a flat Si surface, which was first demonstrated by the formation of alkyl monolayer over both hydrogen passivated (H–Si) Si(1 0 0) and Si(1 1 1) surfaces [2]. Since then, organic functionalization of flat Si surfaces has received intense interest from both materials scientists and engineers, and the efforts have been reviewed many times [3–9]. In comparison with the development of organic functionalization, progress in inorganic modification of flat Si surfaces is lagging. It is noteworthy that coordination and organometallic compounds often possess physical attributes that are desirable for electronic devices, including the ability to store one or more electrons per molecule, to exhibit high spin and function as a single molecule magnet. These useful physical attributes are more difficult to realize in organic species without compromising molecular stability. It is noted that the metal–(coordination compounds)–metal junctions have displayed interesting device characteristics such as the Coulomb blockade, Kondo effect and negative differential resistances [10–13], demonstrating the advantage of both charge flexibility and molecular magnetism of inorganic compounds as the active components. In this contribution, we wish to survey the nascent efforts in covalent modification of flat H–Si surfaces with inorganic species and the preliminary results of electrical and magnetic device studies.

2. Background

The requirement for hybrid devices arises from the need to (a) work within current device fabrication techniques; (b) use existing infrastructure; and (c) develop an understanding of the influence of organic and inorganic species on the local and bulk physical and electronic properties of silicon. The two relevant silicon surface orientations are Si(1 0 0) and Si(1 1 1). Though much research has been based on Si(1 0 0) due to its broad use in industry, Si(1 1 1) is more common in a laboratory setting due to the ease of obtaining an atomically flat hydrogen passivated surface via simple chemical etchings [14–16], which facilitates further modification by "wet" chemistry methods. As Si(1 0 0) is the primary surface used in the micro-electronics industry much of the recent work has focused on this surface, despite the requirement of more stringent preparation procedure. Nevertheless, the surface has been shown to play a minimal role in electron transfer rates and stability characteristics of bound molecules allowing studies using Si(1 1 1) in laboratory settings to be relevant [17]. The most common functionalization is through the formation of a Si–C bond due to the high strength (Si–C, ≈370 kJ) of the bond, while the formation of Si–O bond (Si–O, ≈368 kJ) has been investigated as well. The formation of the Si–C bond results in a more stable system and higher electron transfer rates owing to the less polar nature of Si–C vs. Si–O [4,18]. Molecular passivation of the Si surface can be achieved using two distinct methods: (a) UHV conditions; (b) ambient conditions (wet chemistry technique). The former method has the advantage of being ultra clean and readily integrated with STM and XPS to yield structural details of the passivated surfaces in high precision, but is obviously demanding on infrastructure. The wet technique, on the other hand, requires nothing beyond the setup typical of organic/inorganic synthesis that is accessible to most chemists and biologists. This review will be limited to the passivation performed using wet techniques.

2.1. Bulk silicon

Silicon is an intrinsic semiconductor with an indirect band gap of 1.12 eV and an intrinsic conductivity of $4.3 \times 10^{-6}\ \Omega^{-1}\ cm^{-1}$. To increase the conductivity, group IIIA elements (B, Al, Ga) or group VA elements (P, As, Sb) are used as dopants resulting in *p*- or *n*-type, respectively. The relevant data for Si(1 0 0) and Si(1 1 1) are listed in Table 1.

Table 1
Physical properties of the Si surface [16,19].

	Si(1 0 0)	Si(1 1 1)
Density (atoms cm^{-2})	6.78×10^{14}	15.66×10^{14}
Atomic spacing (Å)	5.43	3.13
Surface energy ($J\ cm^{-2}$)	2.13	1.23

2.2. Surface preparation

Passivation is arguably the most important step for the functionalization of silicon. The surface is most often passivated by hydrogen, though halogens have also been used. Passivation is achieved by etching silicon oxide using HF for Si(1 0 0) and HF or NH_4F for Si(1 1 1), respectively. Using these wet chemical techniques, the surface is rough at the atomic scale containing a mixture of SiH, SiH_2 and SiH_3, which arise from terraces, steps, kinks or vacancies. The surface roughness can be characterized by the hydride formation on the surface with the ideal surfaces of Si(1 0 0) forming SiH_2 and Si(1 1 1) resulting in SiH (Scheme 1). Using either HF or NH_4F to passivate Si(1 1 1) will result in the presence of both SiH and SiH_3, while a mixture of NH_4F and HF results in mostly SiH [4,19].

Prior to passivation, a Si wafer needs to be free of microcontamination, namely ions, metals, hydrocarbons, and particles. The most commonly used cleaning methods are modifications of the RCA process developed in 1970 by Kern and Poutoinen [20]. Photoresist and large particles are removed by solvents (namely acetone, toluene and methanol), and the wafer is then washed in a heated mixture of sulfuric acid and hydrogen peroxide followed by rinsing with ultra-pure water (18 Ω, UP4W) to remove organic contaminants. The initial layer of silicon oxide is then etched by dipping the wafer into an HF solution and rinsing with UPW. The wafer is subsequently placed into a mixture of ammonia hydroxide and hydrogen peroxide, followed by rinsing with UPW to remove many metal contaminants. The etching to obtain a flat Si(1 1 1) surface is then accomplished using either a 1–4% HF solution for 1–2 min, a 40% NH_4F solution for 10–15 min, or a mixture of both solutions. Although NH_4F etching is more time consuming, it is much less haz-

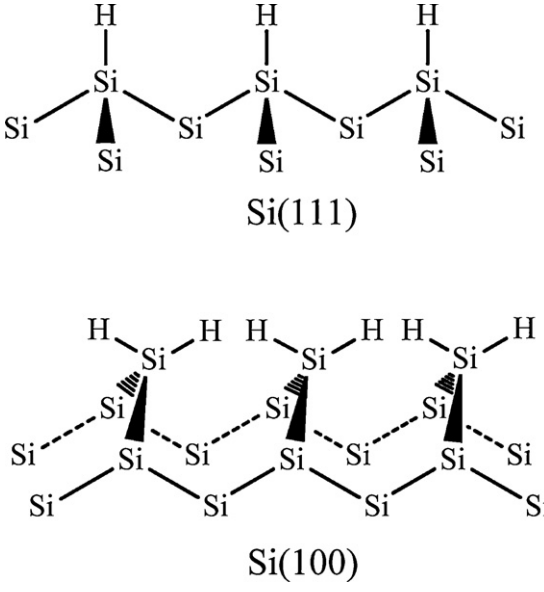

Scheme 1. Idealized hydrogen terminated surfaces.

ardous than HF etching. To obtain a hydride terminated Si(1 0 0) surface, a 1–4% HF solution is required, while the usage of concentrated HF over an extended period of time will result in the formation of porous silicon [4]. For many systems, a simplified and successful method invokes the placement of the wafer in a piranha wash (H_2SO_4:H_2O_2) at 80 °C and UPW rinsing before being etched by either HF or NH_4F.

2.3. Deposition

The common molecular passivation methods via wet techniques include cathodic electrografting (CEG), thermal-, and photo-immobilization [21–24]. In most cases, an unsaturated carbon linker is used to displace the hydrogen on the Si surface; other methods include the use of a diazonium molecule, click techniques on a halogenated surface and ligand displacement [25]. Thermal deposition commonly occurs in the range of 75–200 °C, while some molecules such as porphyrins were deposited by "baking" at temperatures up to 400 °C to form the Si–C/O bond [26]. Photo-immobilization using 254 nm light proceeds via hole-generation on the surface of Si forming a dangling bond, which undergoes a nucleophilic attack by an unsaturated carbon to generate a monolayer. It should be noted that unsaturated carbon compounds can be deposited onto Si in the dark, though to a lower extent (≈10%) [27]. The main methods of characterization for Si surfaces include XPS, FTIR, and cyclic voltammetry (CV). Other methods employed are AFM, SEM, ellipsometry, and β-NMR [28].

2.4. Advantages of inorganic molecules for memory devices

One of the most promising features of hybrid devices is their use in nonvolatile memory technology [29–32], and potential advantages include unique capacitance (charge–voltage) and conductance (current–voltage) characteristics owing to multiple stable redox states that are accessible in a inorganic compound. For instance, while current technology allows for systems with a charge capacitance of 1–2 $\mu C\,cm^{-2}$, the use of porphyrin molecules may lead to devices of capacitance up to 40 $\mu C\,cm^{-2}$ [33]. Furthermore, the charge retention time of porphyrins is on the order of minutes as opposed to tens of milliseconds afforded by current technology [34–36]. An advantage of longer charge retention times is the reduction in the number of refresh cycles, resulting in reduced power consumption. Oxidation/reductions are active processes where a potential is applied to change the oxidation state of a molecule/monolayer; once a potential has been applied, a molecule will be given a charge. The ability to hold the charge without an applied potential is a passive process referred to as charge retention [37]. A second advantage with inorganic compounds is a lower applied voltage is necessary to reduce or oxidize a monolayer relative to current DRAM systems, lowering the device power requirement.

3. Immobilization strategies

3.1. Formation of Si–C bond via hydrosilylation

One of the most efficient functionalization methods for molecular attachment onto Si surface is by the formation of a strong Si–C bond [4]. The Si–C bond is typically formed through deposition of an unsaturated alkene or alkyne onto passivated Si by photo-, thermo-, electrochemical activation, or the use of Grignard reagents. Thermal and photo-depositions are the most commonly applied techniques in regards to the placement of molecules containing transition metals when forming a Si–C bond. Thermal deposition requires elevated temperatures (>100 °C) resulting in a surface radical via homolytic cleavage of SiH bond, which subsequently reacts with the unsaturated C=C bond (Scheme 2). An alternative method to thermal deposition is the application of 254 nm light, which also promotes homolytic cleavage of the SiH bond but at significantly lower temperatures (Scheme 2). After the deposition of an initial layer, multi-layers can be formed by: (1) polymerization via thermal, photochemical, or electrochemical activation; (2) "click" reactions; or (3) substitution reactions.

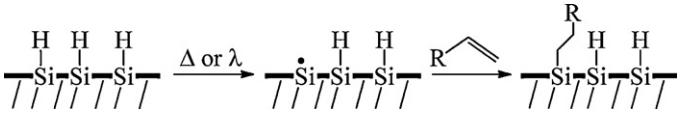

Scheme 2. Radical initiated reactions of H–Si with alkenes.

Ferrocene containing compounds [38,39] are popular candidates for Si surface grafting, which has been achieved with *p*-/*n*-Si(1 0 0) and Si(1 1 1) surfaces (Scheme 3). The first deposition of ferrocene was accomplished with vinylferrocene (**2**) onto *n*-Si(1 0 0) using UHV [22], onto *n*-Si(1 1 1) using thermal deposition [40], and onto both *p*- and *n*-Si(1 0 0) by using visible light from quartz-iodine lamp [41]. Hydrosilylation generally reduces the degree of carbon–carbon unsaturation by one, while alternative methods are employed to maintain the degree of unsaturation. Ethynylferroene (**3**) was deposited onto *p*-Si(1 0 0) in the presence of diethylaluminum chloride resulting in the formation of only a Si–C=C bond [42]. The Grignard reaction between 2-bromoethylferrocene (**1**) and *p*-Si(1 0 0) in the presence of Mg turnings resulted in the $FcCH_2CH_2$ attachment [42–45], and the reaction between lithiated **3** and *p*-Si(1 0 0) yielded the FcC≡C deposition [42,46,47]. The resultant coverage of **3** and **1** were 1.5 and 1.8×10^{13} molecules cm^{-2}, respectively [17,42,48]. Alternatively, ferrocene derivatives have been used to functionalize Si via stepwise modification such as the "click" reaction (described below) as well as a carbodiimide coupling (Scheme 4) [49,50]. Also relevant are molecular compounds containing [M]–C≡C–Si linkage [51], which may serve as the model compound for Si-surface bound inorganic species.

To be incorporated in microelectronic devices, molecular modifiers must be able to withstand the rigorous conditions of fabrication processes. Porphyrins are promising candidates for such purpose as they have undergone thermal deposition at temperatures up to 400 °C while remaining intact; they are a group of frequently studied coordination compounds on flat Si surface

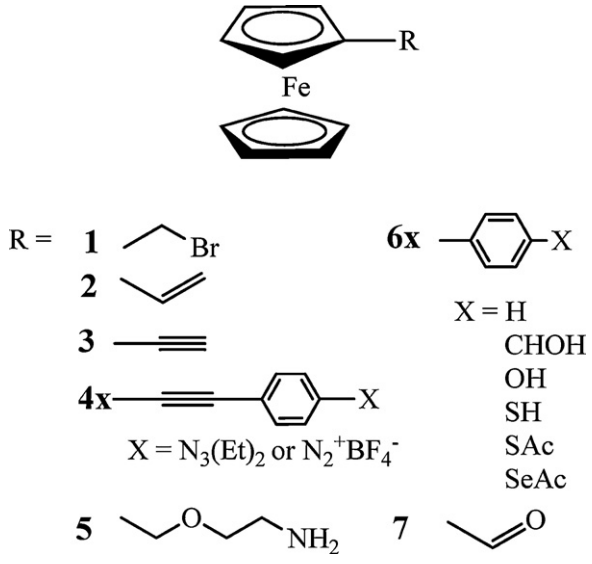

Scheme 3. Ferrocene modified by a variety of linkers.

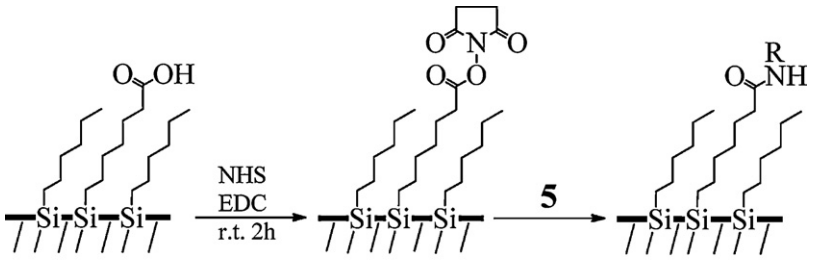

Scheme 4. Functionalization of ferrocene via carbodiimide.

with a few examples being shown in Scheme 5. Demetallation of porphyrins during thermal deposition can occur with the stability order of Co ≈ Cu > Zn as seen from the examples of **15** (see Scheme 5) and **34-OH** (see Scheme 16) [52]. This occurs due to a slightly acidic environment near the Si surface that is attributed to the protons generated by homolytic cleavage of the SiH bonds. In order to increase the stability of metallated porphyrins, pyridine was used as a "proton sponge", which also served to speed up the reaction. Typical surface coverage of porphyrin monolayers bound to silicon by a single tether varies between 3×10^{13} and 6×10^{13} molecules cm^{-2}, corresponding to a molecular footprint of 200–300 $Å^2$ [26,37,53–57]. This is significantly less dense than a complete monolayer as the footprint of a dense porphyrin layer on gold is between 50 and 100 $Å^2$ [58,59]. Using porphyrin containing a tripodal linker, such as **12**, will form three Si–C bonds simultaneously and improve the surface coverage to 1×10^{14}–2×10^{14} molecules cm^{-2} [56,60,61]. In comparison, porphyrins with a bipodal linker that forms two Si–C bonds showed no increase in monolayer density over tethers utilizing a single Si–C bond (monopodal) [62]. Porphyrins bound to Si by a single tether, either monopodal or tripodal, typically display tilt angles of 45 ± 5° to the Si surface [55,60,62]. Tilt angles have been seen as low as 32° such as when the methyl groups in **12-Zn** were substituted with CN [61], but generally do not vary significantly based on the tether or the use of Co, Cu, or Zn for metallation.

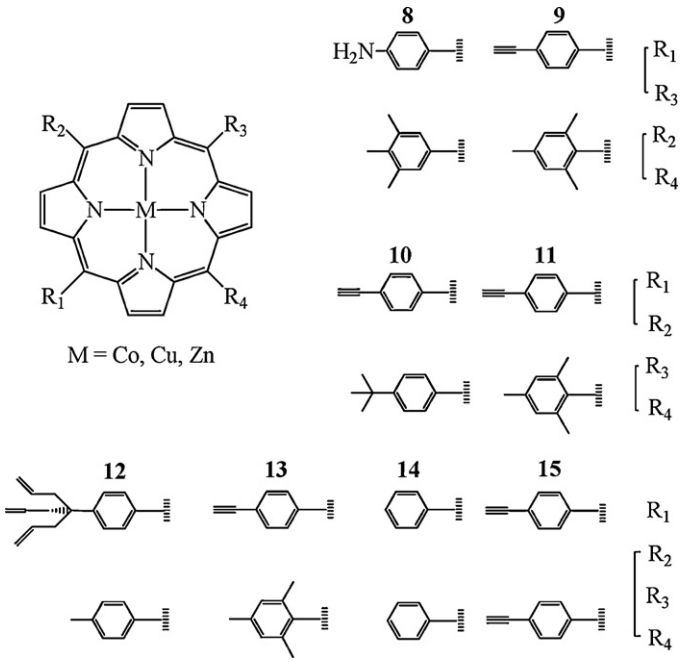

Scheme 5. Porphyrins of various substituents.

A variety of methods have been looked at to further increase the surface coverage of redox active molecules, including multi-layer formation, and direct deposition of multi-porphyrin complexes (Scheme 6) as well as layered growth of porphyrins (Schemes 7 and 8). With two terminal ethyne units in either the *trans*- (**9**), *cis*- (**11**) position, or all four positions (**15**), multi-layers were grown by either increasing solution concentration or deposition time resulting in coverage up to 4.5×10^{15} molecules cm^{-2}; monolayer coverage is around 6×10^{13} molecules cm^{-2} with minimal variation based on the *meso*-substituents of the porphyrin [52,54]. Compounds with four terminal ethyne units (**15**) did result in a lower coverage than those with two ethyne units in the *trans*- or *cis*-positions. One of the main challenges of growing multilayers is obtaining a completely smooth surface with consistent results. To overcome this problem, multi-porphyrin assembly such as **16** was synthesized and subsequently deposited by thermal deposition at 400 °C. This approach led to a surface coverage of **16** around 9×10^{13} molecules cm^{-2} (1.8×10^{14} porphyrin cm^{-2}), and depositions of other porphyrin dyads yielded similar coverage numbers [63].

Triple decker porphyrins (**17**, Scheme 6) based on the combination of porphyrin and phthalocyanine complexed to either Eu or Ce have been placed onto Si(100) [64]. Since these are bulky molecules, the surface coverage is only about 6×10^{12}–1×10^{13} molecules cm^{-2} even with a tripodal tether. The relatively low coverage is partly due to the triple decker porphyrin requiring a large space arising from the ability to rotate around the anchor, which prohibits the attachment of other porphyrins. Rotation was prevented by the use of two tripodal tethers

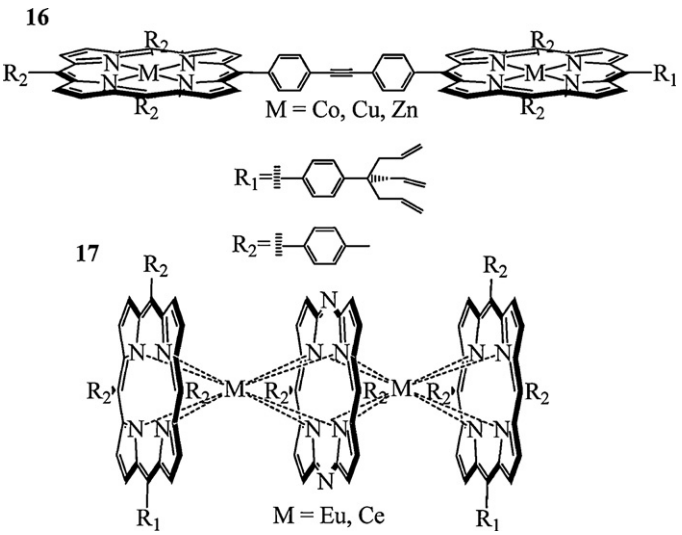

Scheme 6. Preassembled multiporphyrin compounds.

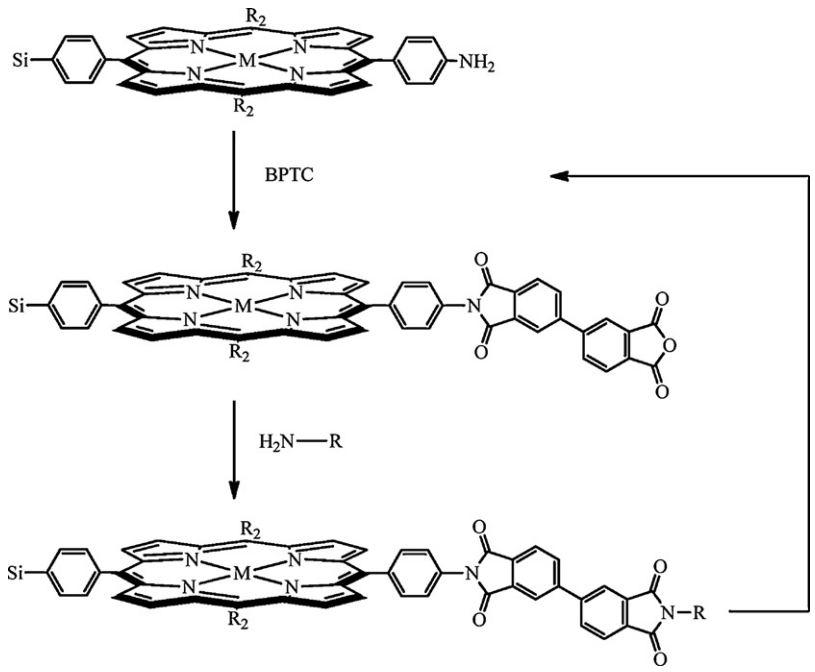

Scheme 7. Substitution pathway resulting in multi-layers.

in the R_1 position, **17**, resulting in an improved coverage up to 5×10^{13} molecules cm^{-2}.

For redox active molecules that cannot be deposited using thermal techniques, alternative methods of forming multi-layers include step-wise growth by substitutions (Scheme 7) and Huisgen cycloaddition chemistry (Scheme 8). Preparation of multi-layers starts with thermal deposition of an initial layer such as **8-Zn**, where the amino-substituent can undergo condensation (Scheme 7) alternating between 3,3′,4,4′-biphenyltetracarboxylic dianhydride (BPTC) and **8-Zn**, which results in multi-layers with coverage up to 3.2×10^{15} molecules cm^{-2} after growth of four layers [65,66]. An alkane chain terminated with either an ethynyl or azido unit can be used to undergo Huisgen-cycloaddition with organometallic species including ferrocene and porphyrin. Using an azido substituted alkane (Scheme 8 – left), both **3**, **13-Zn** have been deposited onto Si(1 0 0) [57,67–69]. Alternatively a terminal alkyne (Scheme 8 – right) bound to Si has been used to attach **14-Ni** containing an azide for the "click" reaction onto Si(1 0 0) [70,71]. Depositions using the "click" reaction yielded similar surface coverage of **3**, **13** and **14** to those from thermal, photo and electrochemical techniques. An added benefit of using the "click" technique is the reduced surface oxidation due to unreacted alkane molecules forming a barrier to O_2 or H_2O.

A variety of other molecules (Scheme 9) have been either directly deposited or reacted with pre-deposited monolayers through ligand exchange (Scheme 10) onto both Si(1 0 0) and Si(1 1 1). Deposition of **18** by either thermal- or photo-deposition and **19** via CEG (cathodic electrografting) onto *n*- and *p*-Si(1 0 0) led to the formation of a dense monolayer, where 2,2′-bipyridine (bipy) complexed to Cu(I) by soaking the functionalized wafer in a $Cu(CH_3CN)_4ClO_4$ solution [72]. The deposition of **19** by CEG resulted in the lowest amount of silicon-oxide present as well as the highest bipy density on the Si surface. Thermal-deposition at 200 °C resulted in the first known deposition of a nickel complex (**25**) onto Si(1 0 0), which is based on the salen ligand [73]. Deposition via ligand exchange is shown in Scheme 10, where a labile ligand on a complex or cluster such as **26** is displaced by an acetate or pyridine type ligand [74]. Coverage tends to be very high with minimal surface oxidation occurring as the initial layer contains densely packed alkane chains. Molybdenum clusters $(Mo_6X_8L_6)^{2-}$, such as **24**, were deposited onto Si(1 1 1) by ligand exchange of pyridine onto a monolayer, where varying ratios of the alkane chain were terminated with 4-pyridine through an amide linkage resulting in a surface coverage of 5×10^{13} molecules cm^{-2} [14,75]. A monolayer containing a mixture of alkane chains terminated with either methyl or carboxyl groups was used to deposit a dodecamanganese cluster, **20**, by ligand exchange with acetate [28,76–79]. The surface coverage of **20** was controlled by varying the concentration of methyl-10-undecenoate in 1-decene during alkane deposition with the coverage of **20** being directly proportional to the amount of methyl-10-undeconoate. Other single molecular magnets (SMMs) that have been deposited onto Si include tetrairon complexes by

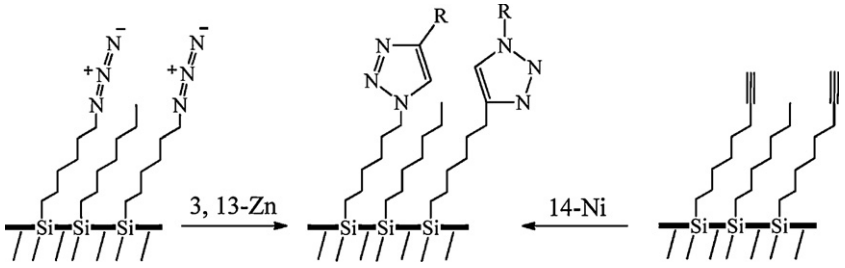

Scheme 8. "Click" reaction used to form layers onto Si.

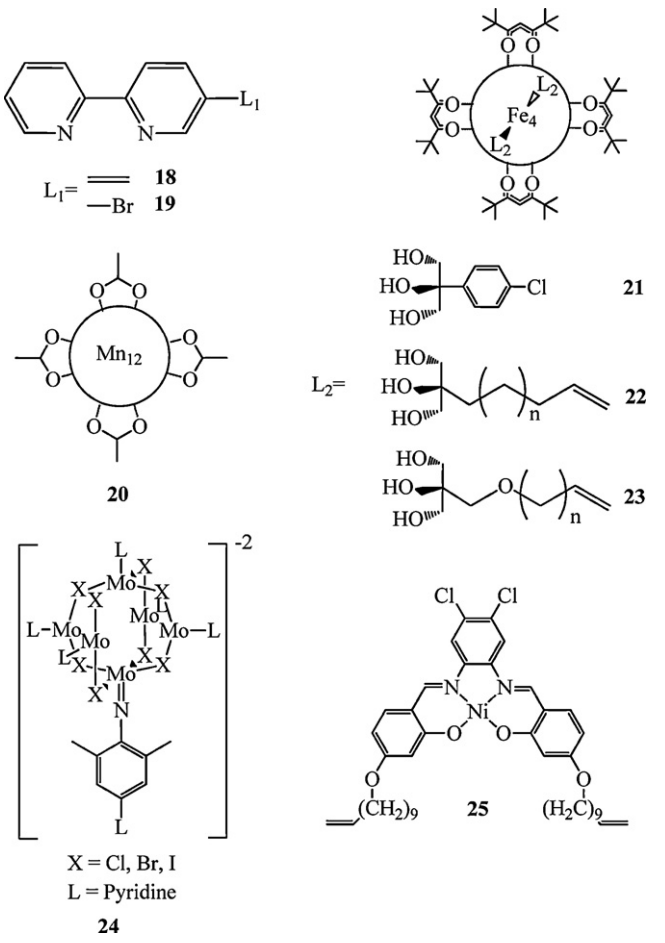

Scheme 9. Complexes for the functionalization of silicon.

ligand exchange (**21**) or photo-deposition (**22** and **23**) [80,81]. The superparamagnetic compound $Cs_{0.7}Ni[Cr(CN)_6]_{0.9}$, a Prussion blue analogue, was deposited via a stepwise pathway utilizing *N*,*N*-bis(pyridin-2-ylmethyl)propane-1,3-diamine to form the initial Ni support, and followed by growth of the CsNiCr nanoparticles onto the Ni support [82,83].

Several different hetero-metallic species have been deposited onto Si including the Keggin-type POM $[PW_9O_{34}(t\text{-}BuSiO)_3Ge(CH_2)_2CONHCH_2C{\equiv}CH]^{3-}$ (**27**, not pictured), which was recently deposited onto highly doped *n*-Si(1 0 0) by CEG [84]. Using photochemical deposition, a variety of iron and ruthenium acetylide complexes containing a terminal acetylene unit (Scheme 11) were bound to *p*-Si(1 1 1) [85]. The surface coverage

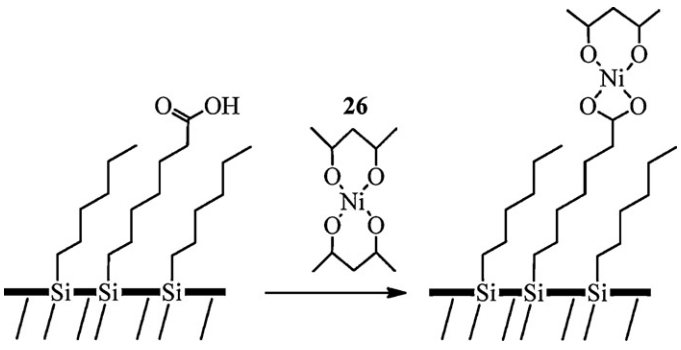

Scheme 10. Deposition of coordination compounds (e.g. **26**) by ligand displacement.

for **28** varied between 9×10^{13} and 1×10^{14} molecules cm^{-2} resulting in a footprint of 90–100 $Å^2$, which is a reasonably dense monolayer as the molecular footprint of **28** is estimated at 65 $Å^2$; increasing the linker length by addition of phenyl units caused minimal variation in surface coverage. The surface coverage of **29**, 6×10^{13} molecules cm^{-2}, was slightly lower than that of **28** due to the steric bulk of the phosphine around the ruthenium core.

3.2. Formation of Si–C bond via diazonium and related species

In addition to alkenes and acetylenes that underwent hydrosilylation reactions with H–Si, aryl diazonium salts facilitate a direct aryl functionalization onto a silicon surface via the formation of Si–C(Ar) bond. Diazonium salt is typically generated from treating an aryl amine with an oxidizing agent such as *t*-BuONO (Scheme 12) [86]. Diazonium salts have been used to deposit organic molecules onto carbon materials including graphite, carbon nanotubes, glassy carbon and diamond; semiconductor surfaces including Si and GaAs; and metals including Fe, Pt, Au, Zn, Ni, Co, Cu, and Pd to name a few [87–90]. At the open circuit potential (OCP) in solution the diazonium salt is reduced to an aryl radical with the concurrent loss of N_2. The radical reacts with Si–H forming a Si–C(Ar) bond (Scheme 12) [91–95]. By applying a negative potential, often around −1 V, the aryl radical is more quickly generated for deposition as well as preventing silicon-oxide growth [91,93]. Due to the thermal or air sensitive nature of diazonium salts, it can be converted to the more robust triazene, from which the diazonium can be generated *in situ* with the use of an acid [95]. Conversion of the triazene to diazonium using HF or NH_4F has the advantage that any SiO_x formed on the surface during functionalization is converted back to H–Si. It should be noted that a minimal amount of acid should be used as many transition metal compounds are unstable in acidic mediums. By adjusting any of the following parameters, time of deposition, concentration of the solution or grafting potential, the amount of material deposited can vary from sub-monolayer to a dense monolayer or multi-layers. This is a convenient approach to obtain a high amount of charge density within a small footprint, providing a pathway towards molecular memory devices based on thermally sensitive molecules [96].

The Tour group carried out extensive work on direct functionalization of both Si(1 0 0) and Si(1 1 1) via diazonium and triazene chemistry using organic and organometallic molecules including porphyrins (**30**), polyoxo-molybdate (**31**) and ferrocene (**4**). By varying the reaction time, the thickness of deposited porphyrin (**30**) ranges from a monolayer in 10 min (3.5 nm, based on a 60° tilt angle, as determined by scanning electron microscopy, SEM) up to 17 layers after 1 h (61 nm based on a 60° tilt angle) [97]. Using a porphyrin containing either Cu (**30-Cu**), Co (**30-Co**), or Zn (**30-Zn**) the reaction time increases significantly due to the lower solubility of metallo-porphyrins, requiring up to 2 h for the formation of a monolayer. Metallo-porphyrins also form multi-layers via radical formation as confirmed in the case of **30-Co**, where SEM showed an average layer thickness of 6.6 nm and a surface coverage of 7.2×10^{14} molecules cm^{-2} [96]. The high obtainable concentration of a porphyrin coupled with two easily accessible oxidation states makes these compounds ideal for memory applications. Another compound that has been investigated for molecular memory devices is ferrocene (see above), of which **4** has been deposited via triazene chemistry leading up to nine layers with a surface coverage of 1.7×10^{15} molecules cm^{-2} (Scheme 13) [98].

A Lindqvist type polyoxo-molybdate (Mo_6O_{19}, **31**, Scheme 12) was modified with an aryl diazonium through the formation of a Mo imido bond [99], and deposited on Si to determine the effect that electron withdrawing groups have on the surface work function and voltage thresholds [100]. The surface coverage of **31** was 1.1×10^{13} molecules cm^{-2} [100], which is rather low compared to

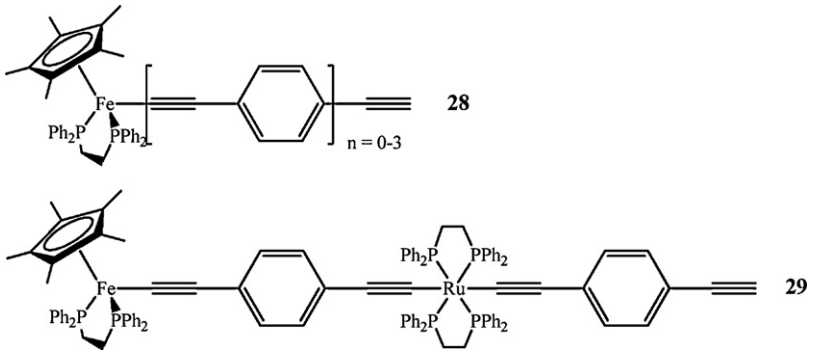

Scheme 11. Homo- and hetero-dinculear oligo(phenyleneethylene) complexes.

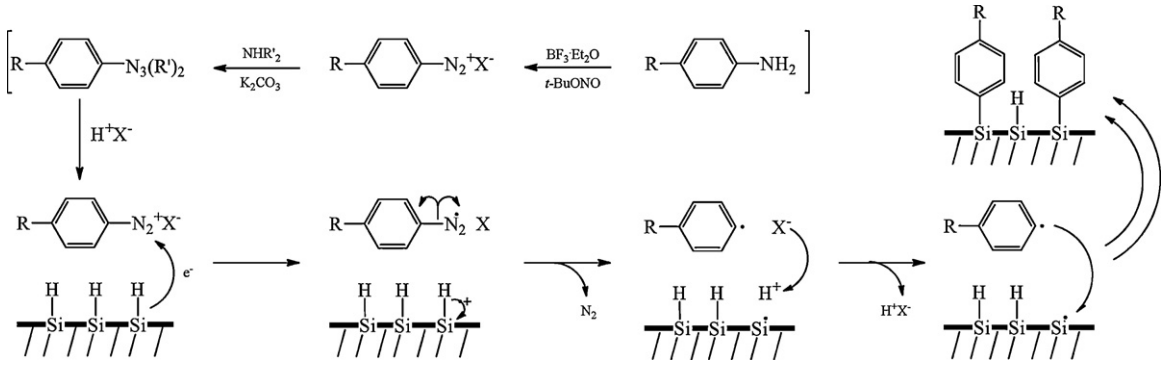

Scheme 12. Radical chain mechanism for the functionalization of Si by molecules containing diazonium or triazene functional groups.

24. Both molecules have low surface coverage because of the bulky nature of the Mo_6 cluster, but **24** had coverage five times as high, 5×10^{13} molecules cm^{-2}. This decreased coverage may also come to some extent from depositing **31** onto Si(1 0 0) vs. Si(1 1 1) as was the case with **24**, highlighting a potential surface coverage disparity between the two different surfaces. Since the direct functionalization of thermally sensitive aryl units can only be obtained via diazonium/triazene chemistry, it may be necessary to perform a multistep functionalization due to (1) a surface bound aryl reacting with a second aryl radical that leads to the uncontrolled growth of aryl oligomers or (2) a secondary functional group reacting with the passivated silicon surface leading to an inverted molecule. Addition of octacarbonyldicobalt to a monolayer containing a terminal alkyne deposited by diazonium resulted in a monolayer containing a Pauson-Khand adduct (**33**, Scheme 14) [96].

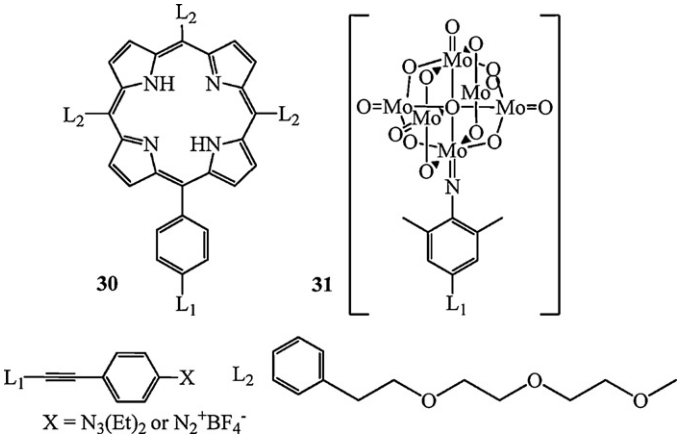

Scheme 13. Porphyrin and molybdenum clusters for deposition via diazonium chemistry.

3.3. Formation of Si–X bond (X = O, N, S or Se)

Several studies have demonstrated the attachment of redox-active molecules onto both Si(1 0 0) and Si(1 1 1) through the formation of either a Si–O–C, Si–S–C, Si–Se–C or Si–N–C covalent linkage [40,41,53,101–104]. Substituted 4-benzyl alcohol (Fz-BzOH, **6-OH**) underwent thermal reactions (70–100 °C) with I–Si [101] and H–Si [103] substrates (Scheme 14) giving a surface coverage of *ca.* 9.0×10^{13} molecules cm^{-2} according to XPS data [101]. It was proven that the resultant surface coverage is directly proportional to the solution concentration of **6-OH**. Functionalization of H–Si(1 0 0 and 1 1 1) with ferrocenecarboxaldehyde (**7** in Scheme 15) was achieved in one step by thermal deposition [40,41]. The prepared interfaces exhibited well-behaved redox characteristics and a linear dependence of current density on the scan rate indicating covalent attachment to the Si surface. The integration of the area under one oxidation/reduction curve of the cyclic voltammograms revealed surface coverage to be 1.5×10^{14} [41] and 1.3×10^{14} molecules cm^{-2} [40] for **7** on Si(1 0 0) and Si(1 1 1), respectively.

Attachment of **34-Zn** has been achieved via Si–O–C, Si–S–C and Si–Se–C linkages onto both Si(1 0 0) and Si(1 1 1) at high temperatures (Scheme 16) [53,101,102]. A triple decker porphyrin similar to **17** using Eu was thermally deposited resulting in coverages between 6×10^{11} and 6×10^{12} molecules cm^{-2} with a thickness of 13–18 Å by varying the concentration of the porphyrin between 2 μM and 2 mM [34,53]. Molecules bound to Si by sulfur or sele-

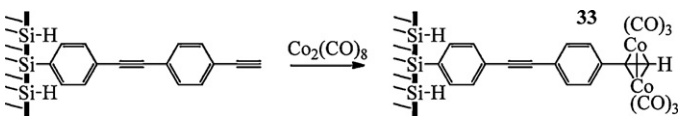

Scheme 14. Use of stepwise diazonium chemistry to form a Pauson-Khand adduct.

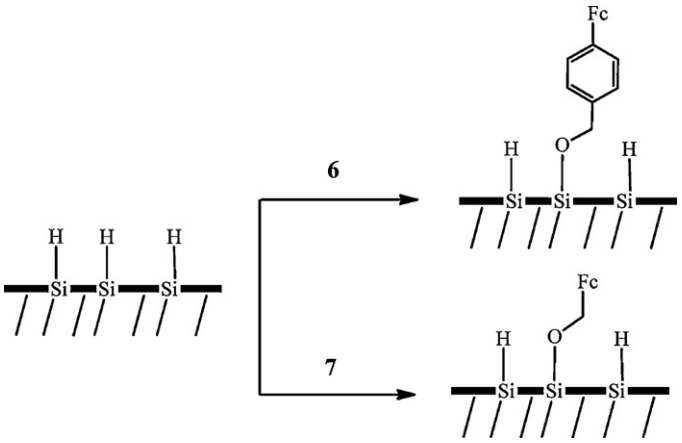

Scheme 15. Functionalization of silicon by ferrocene derivatives via thermal immobilization.

nium exhibited similar electronic properties to those of a Si–O linkage and were nearly as robust, even after extended voltammetric cycling, with stability following the order of O > S > Se [53,102].

Fehlner and co-workers reported the attachment of the bimetallic complex [105] [*trans*-Ru(dppm)$_2$(C≡CFc)(NCCH$_2$CH$_2$NH$_2$)][PF$_6$] (dppm = bis-(diphenylphosphane)methane), **35**, on *p*-Si(1 1 1) through the Si–N–C linker. By placing a chlorine passivated wafer (Cl–Si) into a solution of **35**, the terminal amine reacts with chlorine releasing HCl and binding the nitrogen to two silicon centers to yield a Si$_2$–N–C moiety (Scheme 17). Surface coverage was approximately 4×10^{13} molecules cm^{-2}, corresponding to 45% of the available surface sites. Subsequently, Fehlner and co-workers reported surface functionalization of *trans*-[(H$_2$NCH$_2$CH$_2$C≡N)(dppe)$_2$Ru(C≡C)$_6$Ru(dppe)$_2$(N≡CCH$_2$CH$_2$NH$_2$)][PF$_6$]$_2$, **36**, where only one of the two available terminal amino groups reacted with the Si–Cl surface in a fashion similar to **35** to yield a coverage of 1.6×10^{13} molecules cm^{-2}, corresponding to 15% of available sites [106].

Nalla et al. studied functionalization of a H–Si(1 1 1) surface using the diruthenium carbonyl complex **37**, resulting in the formation of a Si–Ru bond [107]. Photochemical cleavage of the Ru–Ru bond in L$_2$Ru$_2$(CO)$_4$ (L = η^5-MeC$_5$H$_4$, η^5-C$_5$Me$_5$ or HB(pz)$_3$) resulted in the radical species of LRu(CO)$_2$•, which subsequently reacts with the Si–H bond to form a Si–Ru bond (Scheme 18). Evidence of deposition by the Ru moieties onto Si was obtained from FTIR, XPS, and Rutherford backscattering spectrometry (RBS). By

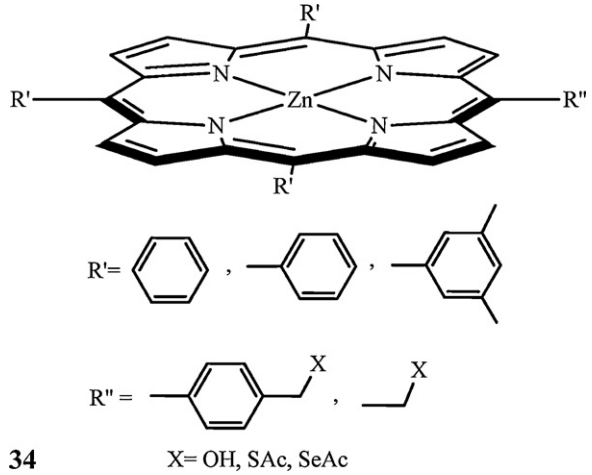

Scheme 16. Porphyrin bound to Si via Si–O–C, Si–S–C and Si–Se–C linkages.

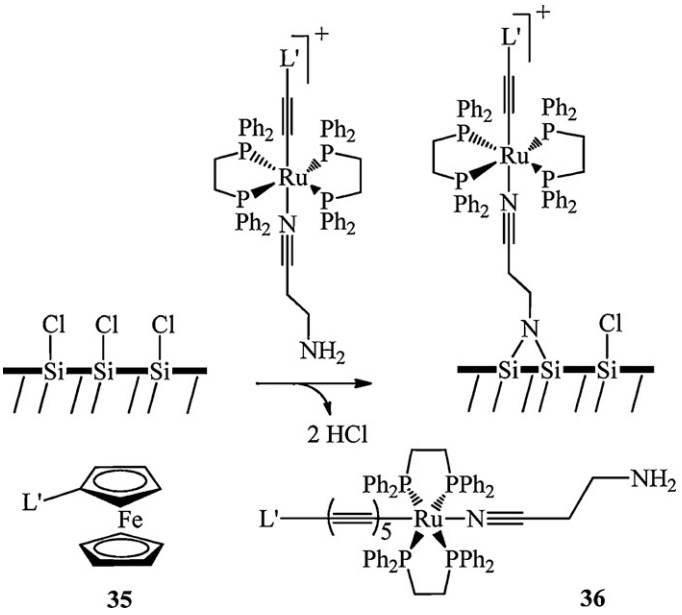

Scheme 17. Reaction of **35** and **36** with Cl–Si(1 1 1) surface to generate a surface bound specie.

the integration of ν(CO) band intensities for the MeCpRu(CO)$_2$–Si the OC–Ru–CO bond angle was estimated to be 98°. This number is consistent with the proposed structure of a surface-confined ruthenium species with two carbonyl groups in the *cis* position. XPS analysis confirmed that Ru(II) was bound to the Si surface. Formation of thin films of metals or binary metal compounds on Si via CVD or ALD method was described in detail in a recent *Concept* paper by Rodríguez-Reyes and Teplyakov [108].

4. Surface characterization techniques and device fabrication

4.1. X-ray photoelectron spectroscopy (XPS)

XPS is one of the most useful techniques for evaluation of the chemical and energetic nature of molecules bound to a surface due to its sensitivity and low detection limit. A representative spectrum is shown in Fig. 1 [4,109,110]. The main purpose of XPS is to determine the presence of a variety of elements (Table 1), their oxidation states when attached to the Si surface and the quality of the deposited layer(s). For functionalization of Si surfaces by the molecules mentioned above, a clean surface needs to be obtained and is represented by a sharp peak at 98.5 eV for Si–H with no detectable silicon oxide, which would appear as a broad peak at 103.3 eV [37]. Most often a small amount of silicon oxide

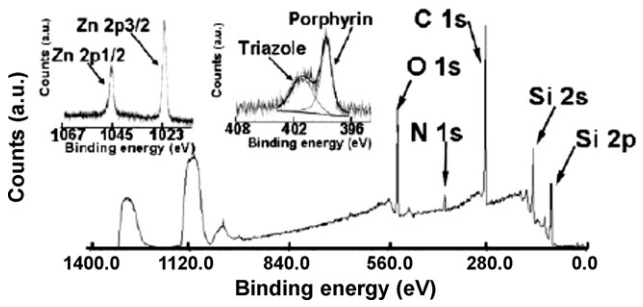

Fig. 1. A representative XPS spectrum of **13-Zn** bound to Si via "click" chemistry. Adapted from Ref. [69].

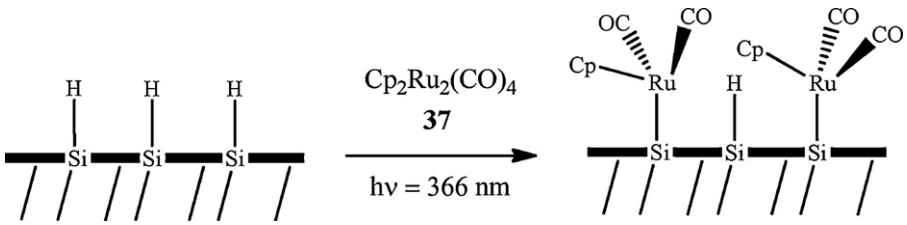

Scheme 18. Surface ruthenation of the Si(1 1 1) wafer by photolysis.

Table 2
Binding energies of various atomic orbitals by XPS.

Atomic center	Binding energy (eV)	Atomic center	Binding energy (eV)
Fe (II) ($2p_{3/2}$)	708–709 [18,68,113]	Mn ($2p_{3/2}$)	641.7 [76]
Fe (II) ($2p_{1/2}$)	720.4 [37]	Ni ($2p_{1/2;\ 3/2}$)	873.8; 856.1
Fe (III) (2p)	711–713 [18,68,113]	N (1s)	398–400 [52]
C (1s)	285–290 [52]	I ($3p_{3/2;\ 1/2}$)	874.1; 930.1 [37]
SiH_x (2p)	99.7 [114]; 98.5 [37]	I ($3d_{3/2;\ 1/2}$)	618.8; 630.5 [37]
SiO_x (2p)	103–104 [68,115]	Zn ($2p_{3/2;\ 1/2}$)	1019.7; 1042.6 [37]
O (1s)	532.1 [37]	Ru ($3p_{1/2;\ 3/2}$)	485, 463 [107]
Br (3d)	70.7 [68]	Co ($2p_{1/2;\ 3/2}$)	781; 796 [116]

and other carbon contaminants can be detected after functionalization even under inert conditions due to the presence of trace amounts of water and hydrocarbons [37,111]. XPS has also been used to determine the ratio of two different molecular species on the same surface [52,97], the formation of metal overlayers on a SAM [61,112] and the thickness of a monolayer. While XPS is almost omnipresent in the study of molecular deposition onto flat Si surfaces, only a few selected examples will be discussed here (Table 2).

For 2,2-bis(hydroxymethyl)-10-undecen-1-ol deposited on Si, four distinct carbon peaks could be discerned in XPS at 283.5 (Si–C), 284.4 (C–C), 287.2 (O–CH_3) and 289.4 eV (C=O), demonstrating the utility of XPS in revealing the presence of a molecule covalently bound to Si [49,76,77,117]. Proving the deposition of **20**, a broadened C=O peak was observed along with the peak at 641.7 eV attributed to Mn; the Si–C bond was not detected due to the increased thickness of the grafted layer [76,77,79]. Furthermore, for the manganese clusters, the average oxidation state of Mn center was the expected value of 3.33 based on peak splitting of the Mn (3s) orbital [79]. Results obtained for nickel compounds **25** and **26** displayed characteristic Ni (2p) peaks at 855.5 and 873.1 eV, revealing the stability of these molecules during deposition [74,117].

XPS of free base porphyrins contain two symmetric and energetically distinct nitrogen peaks at *ca.* 398 (–C=N–, imine) and *ca.* 400 eV (–NH–, pyrrole), while metallation causes the two peaks to merge into one at *ca.* 399 eV [118–124]. The free base porphyrins **8**, **15**, **30** and **34** display two distinct peaks when bound to a Si surface that merged into one peak for a metallated porphyrin as shown in Fig. 2 [52,97]. The ratio between free and metallated porphyrins can be determined based on the comparison of the intensities of the imino (398 eV) and metal coordinated (399 eV) nitrogens. The pyrrole peak (400 eV) does not provide as good of a representation due to the presence of adsorbed nitrogen as well as potential protonation of the imine nitrogen [97,125]. Porphyrin compounds **8-Co**, **15-Cu**, **30-Cu** and **30-Cu** displayed higher amounts of metallated porphyrin on the surface when compared to **30-Zn** or **34-Zn**, the latter of which were partially demetallated by protons generated from homolytic cleavage of the Si–H bond [52,97]. The ratio of nitrogen peaks have also been used in probing the formation of multi-layers shown in Scheme 7, where an increase in the peak ratio of 398.3–400.5 eV was used as an indicator of the increase in porphyrin nitrogens vs. BPTC ligand nitrogens [66]. Two distinct peaks were seen for molybdenum in **31** based on Mo=N and Mo=O, where the 1:5 ratio suggested only monolayer formation [100].

Redox active compounds deposited onto Si may exhibit several oxidation states simultaneously, and in the case of ferrocene both Fe(II) and Fe(III) oxidation states have been detected. The initial deposition of **2** and **3** in acidic medium gives rise to ferrocenium, but in a small quantity compared to ferrocene (*ca.* 1: 15 ratio) [40,98]. After voltammetric cycling, the ratio of Fe(II) to Fe(III) decreased in the process termed "aging". XPS revealed the absence of new anionic species, but rather an increase in silicon oxide that was consistent with the increase of ferricenium [18,126]. Aging is the process that occurs during anodic voltage cycling resulting in an increase of the silicon oxide at sites containing only H–Si or point defects forming silanol, which can then deprotonate and stabilize ferrocenium [18,41,126]. The tetrairon complex **21** was deposited

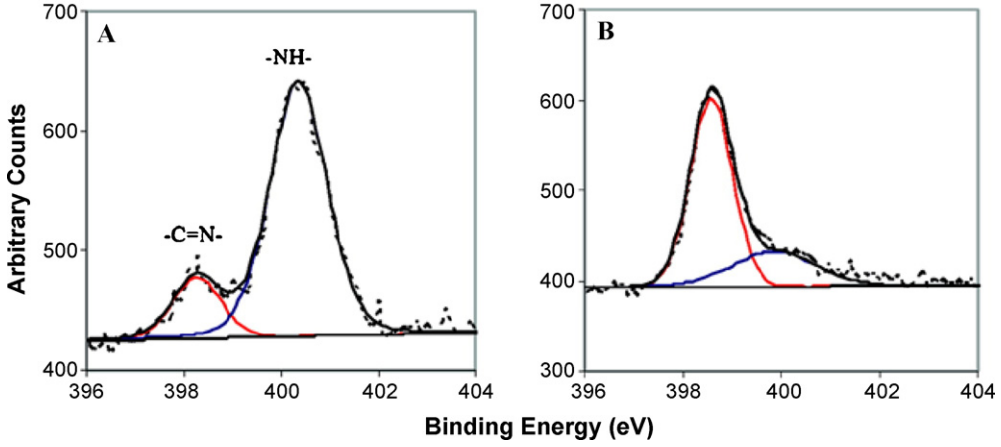

Fig. 2. N (1s) – XPS spectra of porphyrin multilayer on Si(1 0 0): (a) **30** and (b) **30-Cu**.

Adapted from Ref. [97].

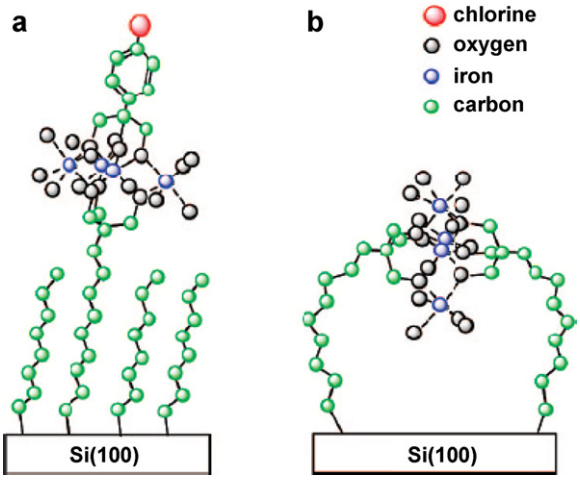

Fig. 3. Potential binding modes of **21**.
Adapted from Ref. [81].

onto the Si surface by varying the concentration of the receptor 2,2-bis(hydroxymethyl)-10-undecen-1-ol and the existence of two different binding modes were detected by XPS (Fig. 3) [80,81]. At low concentration of the receptor (1%), the normalized Cl intensity is half of that for pure **21**, which suggests the attachment of a single receptor (binding mode **a**, Fig. 3). With the pure receptor monolayer, on the other hand, XPS indicates the presence of negligible amount of Cl, which is consistent with the replacement of both 2-(4-chlorophenyl)-2-hydroxymethyl-propane-1,3-diol in **21** (binding mode **b**).

Since the deposition of inorganic compounds onto Si is mainly driven by the search for novel memory devices, it is necessary to form a top contact to yield a metal/molecule/semiconductor hybrid. Metal overlayers have been studied using XPS to determine the quality of the metal layer (e.g. the presence of metal-oxide or contamination) as well as penetration of the metal into the molecular layer [61,112,127]. Hybrid devices were formed by first depositing a monolayer of **12** onto *p*-Si(1 0 0), and subsequently layering with either Cu, Ag, or Au by electron-beam evaporation in UHV. It was determined using XPS that all three metals would penetrate the porphyrin monolayer to form metal filaments with Si if given enough time when sputtering while Au is the fastest in forming filaments. Shown in Scheme 12, **33** was deposited by a well understood reaction to form the Pauson-Khand adduct. Although ellipsometry was unable to detect the minimal change in surface height (<2 Å), XPS clearly revealed the presence of Co with a peak at 780 eV [96].

Under the assumption that a uniform and dense monolayer is formed, the average height of a molecule can be estimated by comparing the ratio of the functionalized silicon to the pure silicon signal (Eq. (1)) [72,111,128,129]:

$$h = -\lambda(E_{Si}\cos(\theta_d)\ln\left(\frac{I_{Si}}{I^{\circ}_{Si}}\right) \quad (1)$$

where $\lambda(E_a)$ is the mean free path of Si (2p) electrons of a given energy ($\approx$ 33 Å) and θ_d is the take off angle. While the diameter of molecule **34-Zn** is 20 Å, a surface height of 18 ± 1 Å was obtained and a tilt angle of 17° was inferred, the latter of which was confirmed by FTIR as discussed below [111]. The Zanoni group used XPS to determine the thickness of silicon oxide formed during the grafting of **18** and **19** using various techniques. Thermal grafting resulted in the most silicon oxide formation, up to 1.3 nm on *n*-Si (a monolayer is 0.25 nm [129]), while CEG had the least oxide formation, 0.1 nm on *p*-Si [72].

4.2. FT-IR

The silicon surface and many deposited molecules have been well characterized by various FT-IR techniques at all stages of passivation and functionalization under various conditions [3,110]. FT-IR is used to determine the functional groups present on a silicon surface. Due to the low molecular concentrations often only intense bands such as C–O stretches are seen. Molecules deposited in a stepwise manner such as the porphyrin shown in Scheme 6 [66] or others via ligand exchange (as shown in Scheme 10) [117] are easily monitored by FTIR due to the presence of a strong C–O and C=O stretches between 1500 and 1700 cm^{-1}, which become either lost or shifted in the subsequent reactions. Alternatively, due to the sheer number of C–H bonds, C–H stretches can be seen between 2700 and 3200 cm^{-1}.

Both transmission and reflectance FTIR techniques have been applied most commonly using lightly doped Si wafers as silicon is optically inert in the infrared region. Heavily doped wafers have also been used, which result in "metal-like" surface-IR selection rules [56]. The most frequently used technique is transmission taken at the Brewster angle (74°) using lightly doped samples. The major downfall of using transmission IR to characterize a monolayer on Si is the very low signal intensity obtained, while the ATR method is capable of yielding a more intense signal. Reflectance spectra are commonly obtained by the ATR method using a germanium crystal due to its high refractivity (GATR utilizes a 65° incident angle). GATR utilizes only a single internal reflection, and to improve the signal to noise ratio as well as use of much larger sample areas multiple internal reflection (MIR-FTIR) has been used with **14** obtaining very high quality results (not shown) [71]. MIR-FTIR utilizes two silicon prisms [130] on which a double-side polished wafer sits on top as shown in Fig. 4. Increasing the separation, *Z*, of the prisms increases the number of reflections that happen within the Si wafer thereby causing an increase of the signal to noise ratio.

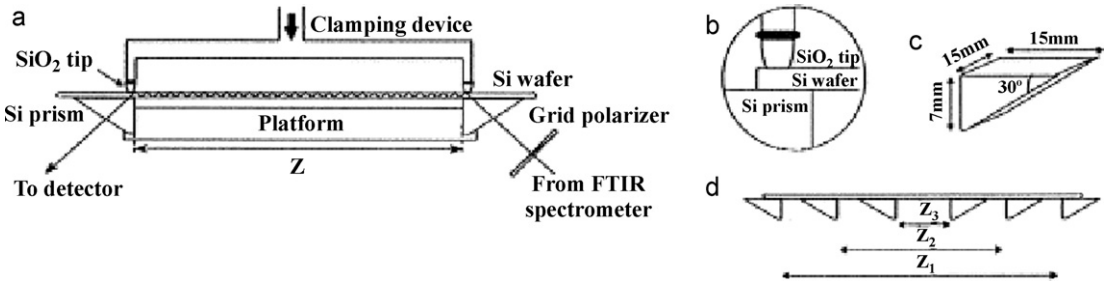

Fig. 4. Salient features of the two-prism MIR geometry: (a) schematic view of the MIR set-up, (b) coupling arrangement for non-destructive measurements, (c) prisms dimensions, and (d) schematic representation of the *Z*-variable experiment.
Adapted from Ref. [130].

One of the most useful applications of FT-IR is the capability to easily extract the tilt angle of a molecule relative to the silicon surface normal. The Bocian and Lindsey groups used FTIR extensively to determine the tilt angle of porphyrins such as **12**, **13**, **14**, and **17** containing Zn, Ni, or Co. Two peaks of importance for porphyrins are the pyrrole "in-plane breathing mode" and the out-of-plane β-pyrrole hydrogen deformation around 998 and 797 cm^{-1}, respectively [56]. By comparing the relative intensities of the two peaks from the reflectance spectra of a pure sample to the transmittance spectra of a deposited monolayer it is possible to extract the tilt angle of a molecule to the surface normal by Eq. (2) or (3).

$$\phi_{tilt} = 1 - \cos^2 \alpha_s - \cos^2 \alpha_{as} \quad (2)$$

$$\frac{A_p^i(R)}{A_\perp^i(R)} = \frac{1}{2}\left[\frac{A_p^i(T)}{A_\perp^i(T)}\right]\left[\frac{\cot^2 \phi}{\sin^2 \theta} + \cot^2 \theta\right] \quad (3)$$

In Eq. (2), α_s and α_{as} are the orientation of the transition dipoles of the symmetric and anti-symmetric vibrations, respectively, and the methodology to obtain these values is beyond the scope of this review [110]. In Eq. (3), A_p^i and $A_\perp^i$ are the absorbance values of the in plane and out of plane pyrrole modes, respectively, for pure (T) and deposited (R) samples. To obtain ϕ using Eq. (3), the rotation angle, θ, is set at 90° by the Bocian and Lindsey groups due to the inability to obtain both values simultaneously [56]. Furthermore, it was determined that the rotation angle of the porphyrin was not uniform and varied between 0° and 90°. The tilt angle of a porphyrin varies between 35° and 55° with the average being around 45°, which agrees with the XPS data discussed above. Tilt angles do not vary much based on the linking unit or metal system, and vary based on the β-substituents by only a few degrees [53,55,56,60–63,65,66,127]. It was determined that the degree of tilt decreases with increasing surface concentration.

4.3. Voltammetry and interfacial charge transfer

Understanding the electrical properties of a monolayer on the silicon surfaces is crucial for the development of molecular-based devices with potential applications including electrical memory, sensors and transistors [31,37,131]. The electrochemical characteristics of monolayers and hybrid devices have been studied by cyclic voltammetry (CV) and electrochemical impedance spectroscopy (EIS).

CV scans are performed to determine the density, quality and rate of electron transfer of monolayers and multilayers. Surface species that are covalently bound have (i) minimal differences between the peak potentials of forward and backward sweeps ($\Delta E_p = E_{for} - E_{back} \sim 0$); (ii) equal current of forward and backward waves ($i_{back} = i_{for}$); (iii) a peak current that has a linear dependence on scan rate.

CVs for monolayers on Si are normally obtained using a general three-electrode system (Fig. 5), but have also been obtained using an electrolyte–molecule–silicon (EMS) setup. Mixed monolayers of **6-OH** and **34-OH** on *p*-Si displayed robust and reversible voltammetric behaviors. Their cyclic voltammograms (Fig. 6) are representative of species that are covalently bound to Si surfaces [131], where the bottom peaks are associated with oxidation (negative current density) and the top peaks with reduction (positive current density) processes. One redox state was detected for **6-OH** (at −0.35 V vs. Ag wire), while two stable redox states were observed for **34-OH** at −0.70 V and −1.05 V.

By varying the scan rates of a mixed monolayer containing **6-OH** and **34-OH** in a ratio of 1:1.4 (Fig. 7), the peak currents scaled linearly, indicating that the electron transfer process occurs within the surface-bound species. Once the applied scan rate exceeds the electron transfer rate, the current starts lagging behind and causes an increase in ΔE_p. For **6-OH** on Si(1 0 0), the peaks were observed to be symmetrical up to 100 V s^{-1} (Fig. 7a), indicating the fast nature of electron transfer. The surface concentration of an attached species, Γ (mol cm^{-2}), can be calculated by using the scan rate dependence of the anodic and cathodic peak currents described in Eq. (4) or by directly integrating the voltammetric waves [132]:

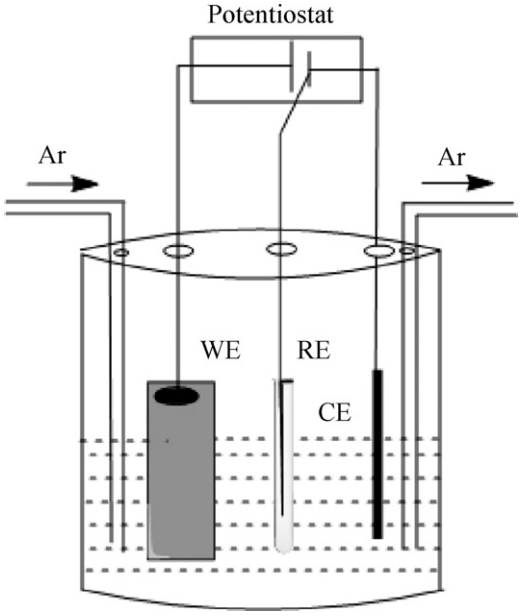

Fig. 5. Schematics of a three-electrode electrochemical setup with modified Si wafer as the working electrode (WE), a reference electrode (RE) and a counter electrode (CE).

$$I_{peak} = \frac{n^2 F^2 \upsilon A \Gamma}{4RT} \quad (4)$$

In Eq. (4), n is the number of electrons; F is Faraday's constant; υ is the scan rate (V s^{-1}); A is the electrode surface area (cm^2); R is the gas constant (J K^{-1} mol^{-1}); and T is the temperature (K). The surface coverage were estimated to be 2.3×10^{13} and 1.0×10^{13} molecules cm^{-2} for **6-OH** and **34-OH**, respectively, with similar results obtained for comparable systems [37,53,55,101,111].

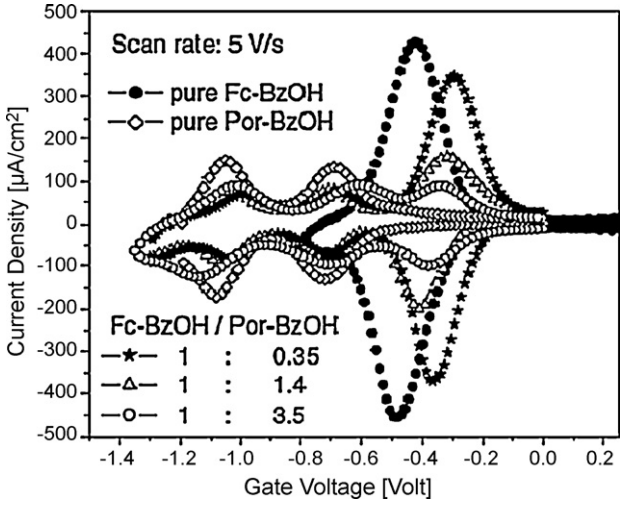

Fig. 6. Cyclic voltammograms of **6-OH**, **34-OH** as pure and mixed monolayers on Si(1 0 0).
Adapted from Ref. [131].

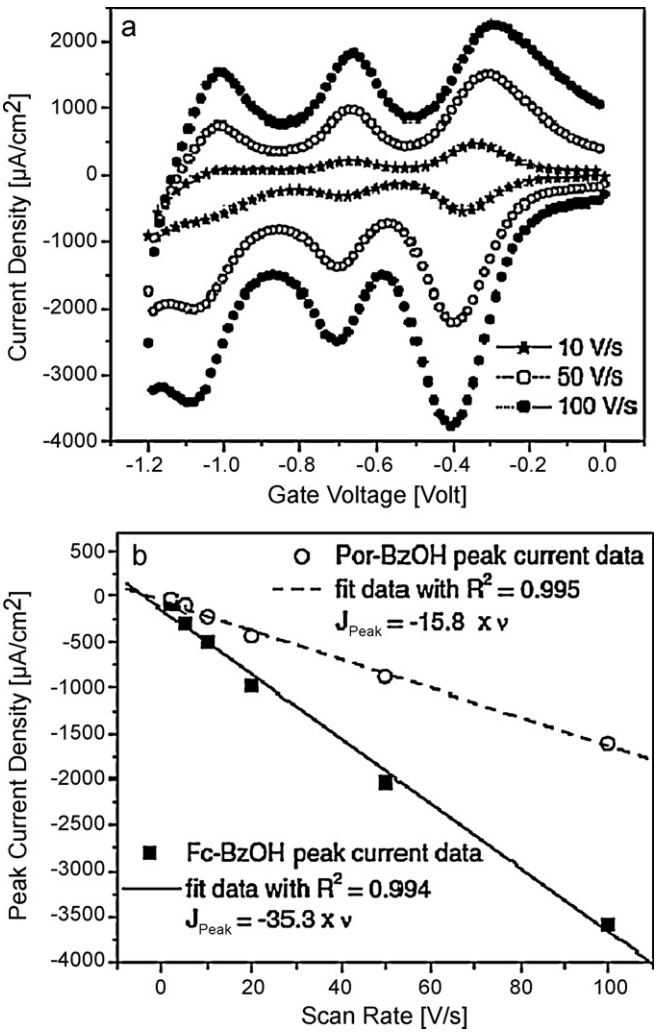

Fig. 7. (a, top) CVs of **6-OH** and **34-OH** in a 1:1.4 molar ratio at scan rates of 10, 50, and 100 V s^{-1} and (b) peak current density as a function of CV scan rate of **6-OH** and **34-OH**.
Adapted from Ref. [131].

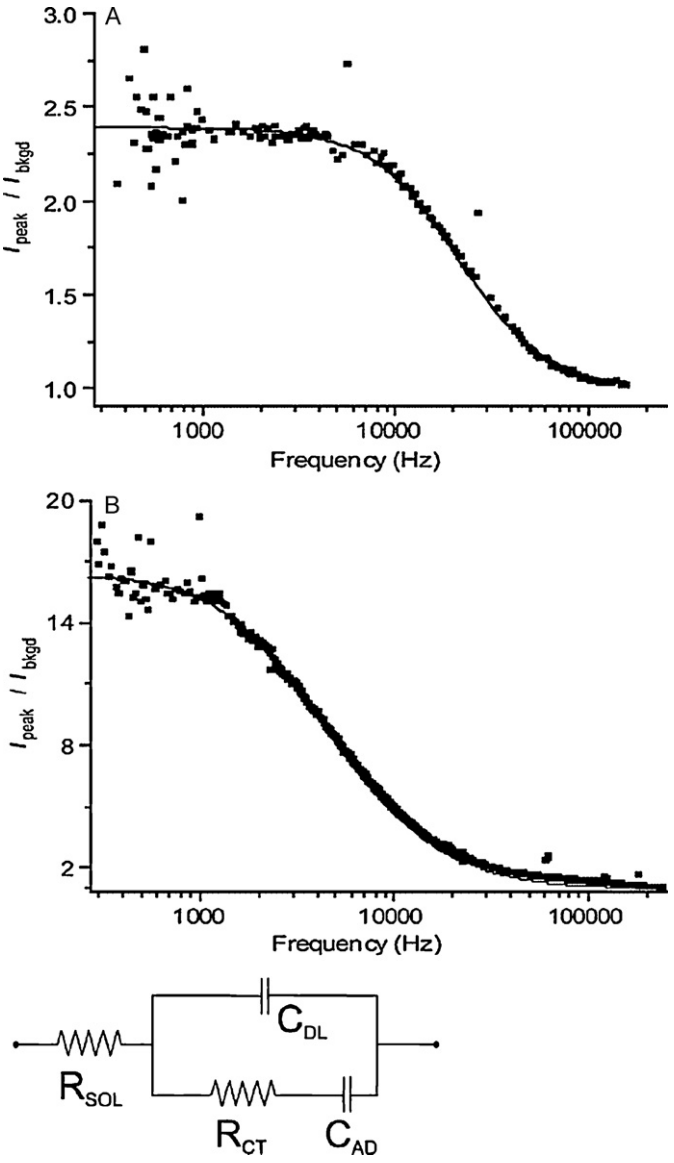

Fig. 8. (a, top) I_{peak}/I_{bkgd} vs. frequency for **6-OH** (A) and **34-OH** (B) on Si(1 0 0); the solid lines represent best fit to the data using a Randles equivalent circuit; Adapted from Ref. [37]. (b) A Randles equivalent circuit for the impedance of an electrode coated with a redox-active monolayer film. Adapted from Ref. [134].

For many examples of monolayers on Si described herein it was possible to determine the standard rate constant of electron transfer, k_0, from the surface bound molecule to the Si surface with techniques including (i) cyclic voltammetry using Laviron's approach [18,41,68,98], (ii) alternating current (AC) voltammetry [37,53,111] and (iii) chronoamperometry (CA) [126]. According to the Laviron method that is based on classical Butler–Volmer theory, k_0 is calculated from Eq. (5) [133]:

$$k_0 = \frac{\alpha n F \upsilon_c}{RT} = (1-\alpha)\frac{nF\upsilon_a}{RT} \quad (5)$$

where υ_c and υ_a are the cathodic and anodic scan rates at $E_p = E^0$, respectively (V s^{-1}); α, the transfer coefficient (a measure of the symmetry of the energy barrier of the redox reaction), is 0.5. Using this approach, k_0 for **2** was 130 s^{-1} [126].

Creager and Wooster developed a method for the determination of the rate constant of electron transfer using AC voltammetric technique [134]. In this method, AC voltammograms are collected in a broad range of frequencies (ω in Hz). The ratio of the peak current (I_{peak}) to the background current (I_{bkgd}) is recorded for each frequency, and the ratio I_p/I_{bkgd} obtained is plot against either ω or log(ω). A representative plot of I_p/I_{bkgd} vs. ω for **6-OH** and **34-OH** deposited onto *p*-Si(1 0 0) is shown in Fig. 8 [37]. The k_0 values are extracted by fitting the plot to a Randles equivalent circuit model (Fig. 8) and determined from Eq. (6). The following parameters are needed to determine the rate of electron transfer: (a) double layer capacitance, C_{DL}, (b) charge transfer resistance, R_{CT}, (c) solution electrolyte resistance, R_{SOL}, and (d) adsorption pseudocapacitance, C_{AD}, which are found from the Eq. (5) presented below. The required input parameters such as C_{DL}, Γ, A, R_{SOL} are obtained from CV and electrochemical impedance spectroscopy (EIS) [101,127]. The electron transfer rate is usually faster at low surface concentrations than at high monolayer concentrations. For example, k_0 for **34-Zn** at low surface coverage ($\Gamma \approx 3 \times 10^{12}$ molecules cm^{-2}) is in the order of 10^5 s^{-1}, while at higher concentration ($\Gamma \approx 1.0 \times 10^{13}$ molecules cm^{-2}) the rate is reduced significantly to 10^4 s^{-1} [53] with similar results being seen for ferrocene [135]. For **6-OH** and **34-OH**, k_0 was 4.5×10^4 s^{-1} ($\Gamma \approx 7.8 \times 10^{11}$ molecules cm^{-2}) and 9.0×10^3 s^{-1} ($\Gamma \approx 1.0 \times 10^{13}$ molecules cm^{-2}), respectively, which was attributed to the difference in surface concentration rather than the nature of redox centers (ferrocene vs. porphyrin) [37].

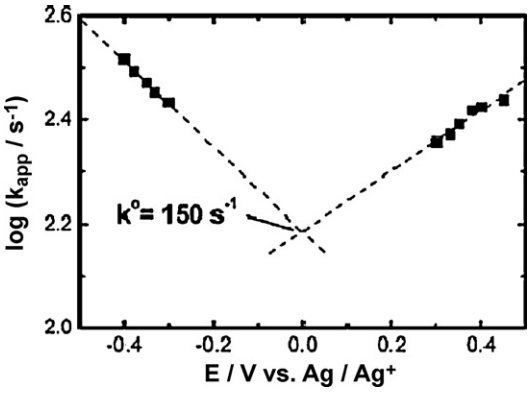

Fig. 9. Logarithmic plot of the k_{app} values vs. potential for **2** on *p*-Si(1 0 0). Adapted from Ref. [126].

$$C_{DL} = \left(\frac{C}{A}\right) A$$
$$C_{AD} = \left(\frac{F^2 A\Gamma}{4RT}\right)$$
$$R_{sol} = \left(\frac{1}{4\pi r_0 k}\right) \quad (6)$$
$$R_{CT} = \left(\frac{2RT}{F^2 A\Gamma k_0}\right)$$
$$k_0 = \left(\frac{1}{2R_{CT}C_{AD}}\right)$$

The electron-transfer rate constant can also be evaluated using chronoamperometry. In such experiments, the apparent rate constant, k_{app}, was obtained by plotting the slope of the curve ln(I) vs. t according to the procedure described by Faulkner et al. [126,136]. Subsequently, log(k_{app}) was plotted against the potential (E), and k_0 obtained from the intercept of the straight lines according to the classical Butler–Volmer theory (Fig. 9). The k_0 value for **2** was 150 s^{-1}, which is in good agreement with Laviron's approach [126].

Electrochemical impedance spectroscopy (EIS) measures interfacial impedance as a function of frequency and has been used in studies of the resistance and capacitance of surface monolayers and their interfaces [101,127]. Impedance measurements involve the application of a sinusoidal AC oscillating voltage to characterize signal response as a function of frequency and DC potential to an electrochemical cell. Typically amplitudes of 5 mV or less are employed in AC measurements, thus inducing minimal disturbance to the monolayer (in comparison, voltammetry typically requires voltage variations across hundreds of millivolts, which may cause modifications in the monolayer structure and composition). Analysis of impedance data in a wide range (25 Hz–5 kHz) provides an enhanced sensitivity and a complete picture of the electrical properties of the system, including capacitance and resistance. The capacitive memory works on the principle of charging and discharging molecules into different reduced or oxidized states. The peaks seen on the capacitance–voltage (*C*–*V*) characteristics are attributed to the charging/discharging transient currents associated with the oxidation/reduction of molecules (Fig. 10) [131] and no peak is observed in the case of a redox-inert monolayer such as with 1-octadecene [57,69]. As the frequency increases (or time constant decreases) beyond the electron transfer rate constant, the redox reaction is unable to keep up with the rapidly changing potential and the peak size diminishes in a similar fashion to MOS capacitors.

The charge retention time of a molecule can be judged from the peak shape of the *C*–*V* curve where a broadened peak indicates some degree of charge loss and a short charge-retention time. The

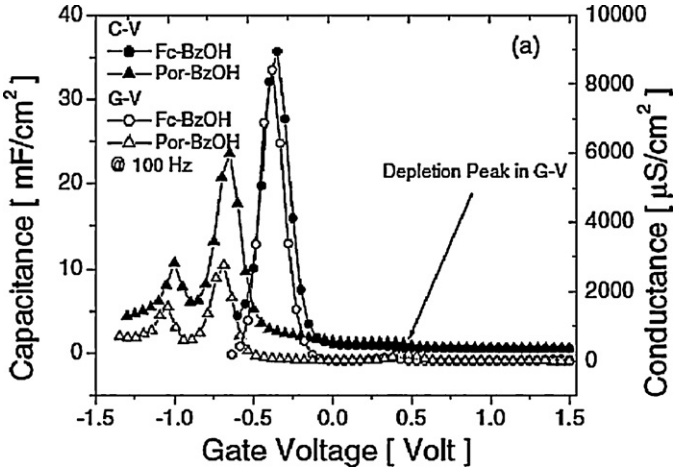

Fig. 10. Capacitance–voltage and conductance–voltage characteristics of monolayer of pure **6-OH** or pure **34-OH**.
Adapted from Ref. [131].

charge-retention time can be prolonged by increasing the length of the linker as well as surface concentration. As demonstrated with **13-Zn** immobilized directly on the surface and alternatively by a $(CH_2)_{11}$ linker the charge retention time increased with the increased linker length as seen in Fig. 11 [57]. Using **34-Zn**, the charge retention time was as low as 10 s when the surface coverage was 6×10^{12} molecules cm^{-2} but increased to 200 s when the surface was saturated at 1.2×10^{14} molecules cm^{-2} [60].

4.4. Others

Complementary methods that are employed include AFM, SEM, ellipsometry and even NMR. These techniques are useful for determining of the presence of monolayers on the Si surface. Other methods that have been used, though sparingly, include ultraviolet photoelectron spectroscopy (UPS), inverse photoemission spectroscopy and the Kelvin Probe, which were used to test the band bending and changes of other electronic properties at the silicon surface by the deposition of various electron withdrawing and donating molecules [25,137]. The thickness of a monolayer on Si can be determined by ellipsometry alone or in conjunction with XPS and SEM [49,97,138]. While ellipsometry is an inexpensive method to quickly determine the thickness and quality of a monolayer, it is

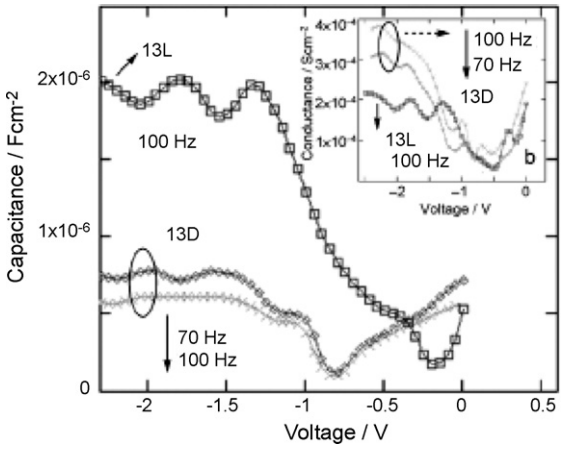

Fig. 11. A *C*–*V* test for ZnEPMP = zinc(II)-5-(4-ethynylphenyl)-10,15,20-trimesitylporphyrin directly grafted (13D, 70 and 100 Hz) and grafted with a linker (13L, 100 Hz).
Adapted from Ref. [57].

unable to detect small changes, as was the case with the deposition of **33** where the addition of Co resulted in a change <2 Å [96].

AFM is most useful for determining the roughness of a surface making it particularly useful for detecting the presence of cluster molecules such as dodecamanganese and other SMMs (single molecule magnets) [14,76,77,79]. A monolayer of SMMs provides very little magnetic material and the magnetic properties become impossible to determine using standard techniques such as SQUID (superconducting quantum interference device). β-NMR is a new technique that provides an increase in sensitivity on the order of 10^{13} by measuring the resonance of ^{8}Li [139–143]. β-NMR has been successfully applied to a monolayer of dodecamanganese in the temperature range of 3.2–130 K. The magnetic properties of a monolayer were significantly different than in bulk material, likely due to changes in the electronic structure resulting from interactions of the Mn_{12} core with the Si surface [28].

4.5. Devices

To our knowledge, there is only one study of a hybrid junction fabricated from an inorganic compound on the Si surface [61]. After the deposition of **12-Zn** onto Si(1 0 0), a metal layer was formed using electron-beam evaporation of Cu, Ag, and Au of thicknesses ranging from 3 to 30 nm. By performing electrochemical measurements of a sample with a metal overlayer in an aqueous system, a signal corresponding to **12-Zn** was detected with either Cu or Ag as the overlayer of up to 8 nm thickness, suggesting incomplete coverage. With a Au overlayer as thin as 1.5 nm, there was a complete loss of signal of **12-Zn**, signifying that Au forms a filament directly with the Si substrate. On the other hand, the metal penetration by Ag and Cu was minimal, suggesting their possible use for hybrid devices.

It has been revealed that porphyrins, metallocene, SMMs and triple-decker coordination compounds: (a) offer the possibility of multibit storage at relatively low potentials (below 1.6 V); (b) undergo numerous (trillions) of write/read/erase cycles; (c) exhibit long charge retention times (minutes); and (d) provide significantly increased charge density [34,41,53,64,101,111]. Most porphyrin molecules provide two easily accessible oxidations providing the option for multibit memory. The multibit system can be further improved with the use of mixed monolayers [131], where **6-OH** and **34-OH** containing Zn were deposited in varying ratios to provide three easily accessible oxidation states. Furthermore, the charge density of inorganic systems is significantly higher than current dynamic random access memory of 1–2 $\mu C\,cm^{-2}$, where charge densities of up to 35 $\mu C\,cm^{-2}$ have been obtained using **12-Zn** [61,66].

5. Outlook

Given the rich variety of reactions the H–Si surface may undergo and interesting electrical and magnetic properties of surface-bound inorganic compounds may bring about, efforts described in this review are merely the proverbial "tip of iceberg". In terms of reaction chemistry, the H–Si surface can be easily converted to X–Si surface (X = halides and azide), the latter of which may undergo the Grignard, cross-coupling or *click* reactions and hence open the door to a broad spectrum of inorganic modifiers. For instance, a microwave assisted Sonogashira coupling reaction between arylethyne and a Si surface-bound Ar–I was realized recently [144], revealing cross-coupling reactions as a mild pathway for molecular passivation of the Si surface. It has been shown that single molecule magnets are typically clusters self-assembled in solution, such as Mn_{12} and Prussian blue analogues [82,145]. It is conceivable to first immobilize a supporting ligand on the Si surface, and then proceed to the assembly of a single molecule magnet cluster on the surface.

Inherently challenging is the characterization of monolayers beyond simple imaging, and new technologies are necessitated to quantify the electrical and magnetic responses of two dimensional assemblies, a sentiment that was expressed in a recent review on magnetism [146]. Scanning tunneling microscopy (STM) is a powerful tool in revealing the packing modes and domain formation of molecular monolayers on Au [147,148]. However, probing a molecular layer on Si using STM has been limited to site-selective passivation under UHV conditions [8], while extension of STM studies to large areas of molecular layers on Si prepared using wet chemistry methods remains to be desired. Furthermore, effective remedies are needed to form a metal overlayer without compromising the molecular layer, which is the bottleneck to fabricate metal–molecule–silicon devices. For instance, indirect and low energy deposition of Au was demonstrated to yield high quality Au/molecule/GaAs junctions [149]. Finally, a standardized protocol that is universally applicable in measuring the *I–V* or electrochemical characteristics of both the molecule–Si and metal–molecule–silicon junctions is sorely missing. This issue is unfortunately prevalent in all areas of molecular electronics [150], and its solution will undoubtedly accelerate the maturation of the field.

Acknowledgements

We thank the support from both Purdue University and National Science Foundation (CHE 0715404).

References

[1] International Technology Roadmap for Semiconductors: Executive Summary. http://www.itrs.net/Links/2009ITRS/2009Chapters_2009Tables/2009_ExecSum.pdf, 2009.
[2] M.R. Linford, C.E.D. Chidsey, J. Am. Chem. Soc. 115 (1993) 12631.
[3] S.F. Bent, Surf. Sci. 500 (2002) 879.
[4] J.M. Buriak, Chem. Rev. 102 (2002) 1271.
[5] D.K. Aswal, S. Lenfant, D. Guerin, J.V. Yakhmi, D. Vuillaume, Anal. Chim. Acta 568 (2006) 84.
[6] Z. Ma, F. Zaera, Surf. Sci. Rep. 61 (2006) 229.
[7] T.R. Leftwich, A.V. Teplyakov, Surf. Sci. Rep. 63 (2008) 1.
[8] M.A. Walsh, M.C. Hersam, Ann. Rev. Phys. Chem. 60 (2009) 193.
[9] A. Vilan, O. Yaffe, A. Biller, A. Salomon, A. Kahn, D. Cahen, Adv. Mater. 22 (2010) 140.
[10] J. Park, A.N. Pasupathy, J.L. Goldsmith, C. Chang, Y. Yaish, J.R. Petta, M. Rinkoski, J.P. Sethna, H.D. Abruna, P.L. McEuen, D.C. Ralph, Nature 417 (2002) 722.
[11] W.J. Liang, M.P. Shores, M. Bockrath, J.R. Long, H. Park, Nature 417 (2002) 725.
[12] H.B. Heersche, Z. de Groot, J.A. Folk, H.S.J. van der Zant, C. Romeike, M.R. Wegewijs, L. Zobbi, D. Barreca, E. Tondello, A. Cornia, Phys. Rev. Lett. 96 (2006).
[13] A.K. Mahapatro, J. Ying, T. Ren, D.B. Janes, Nano Lett. 8 (2008) 2131.
[14] S. Ababou-Girard, S. Cordier, B. Fabre, Y. Molard, C. Perrin, ChemPhysChem 8 (2007) 2086.
[15] D.D.M. Wayner, R.A. Wolkow, J. Chem. Soc., Perkin Trans. 2 (2002) 23.
[16] X.G. Zhang, Electrochemistry of Silicon and Its Oxide, Kluwer Academic/Plenum Publishers, New York, 2001.
[17] A. Boccia, F. Decker, A.G. Marrani, S. Stranges, R. Zanoni, M. Cossi, M.F. Iozzi, Superlattices Microstruct. 46 (2009) 30.
[18] R. Zanoni, F. Cattaruzza, C. Coluzza, E.A. Dalchiele, F. Decker, G. Di Santo, A. Flamini, L. Funari, A.G. Marrani, Surf. Sci. 575 (2005) 260.
[19] R.E. Johnson, R.H. Dettre, D.A. Brandreth, J. Colloid Interf. Sci. 62 (1977) 205.
[20] W. Kern, D.A. Poutoinen, RCA Rev. 31 (1970) 187.
[21] J.M. Buriak, Chem. Commun. (1999) 1051.
[22] P. Kruse, E.R. Johnson, G.A. DiLabio, R.A. Wolkow, Nano Lett. 2 (2002) 807.
[23] M.R. Linford, P. Fenter, P.M. Eisenberger, C.E.D. Chidsey, J. Am. Chem. Soc. 117 (1995) 3145.
[24] M.P. Stewart, J.M. Buriak, J. Am. Chem. Soc. 123 (2001) 7821.
[25] T. He, J. He, M. Lu, B. Chen, H. Pang, W.F. Reus, W.M. Nolte, D.P. Nackashi, P.D. Franzon, J.M. Tour, J. Am. Chem. Soc. 128 (2006) 14537.
[26] Z.M. Liu, A.A. Yasseri, R.S. Loewe, A.B. Lysenko, V.L. Malinovskii, Q. Zhao, S. Surthi, Q.L. Li, V. Misra, J.S. Lindsey, D.F. Bocian, J. Org. Chem. 69 (2004) 5568.
[27] R.L. Cicero, M.R. Linford, C.E.D. Chidsey, Langmuir 16 (2000) 5688.
[28] Z. Salman, K.H. Chow, R.I. Miller, A. Morello, T.J. Parolin, M.D. Hossain, T.A. Keeler, C.D.P. Levy, W.A. MacFarlane, G.D. Morris, H. Saadaoui, D. Wang, R. Sessoli, G.G. Condorelli, R.F. Kiefl, Nano Lett. 7 (2007) 1551.
[29] J.C. Scott, L.D. Bozano, Adv. Mater. 19 (2007) 1452.

[30] R. Waser, M. Aono, Nat. Mater. 6 (2007) 833.
[31] Q.L. Li, Mod. Phys. Lett. B 22 (2008) 1183.
[32] F. Duclairoir, L. Dubois, A. Calborean, A. Fateeva, B. Fleury, A. Kalaiselvan, J.C. Marchon, P. Maldivi, M. Billon, G. Bidan, B. de Salvo, G. Delapierre, J. Buckley, K. Huang, R. Barattin, T. Pro, Int. J. Nanotechnol. 7 (2010) 719.
[33] J.A. Mandelman, R.H. Dennard, G.B. Bronner, J.K. DeBrosse, R. Divakaruni, Y. Li, C.J. Radens, IBM J. Res. Dev. 46 (2002) 187.
[34] Z.M. Liu, A.A. Yasseri, J.S. Lindsey, D.F. Bocian, Science 302 (2003) 1543.
[35] D. Gryko, J. Li, J.R. Diers, K.M. Roth, D.F. Bocian, W.G. Kuhr, J.S. Lindsey, J. Mater. Chem. 11 (2001) 1162.
[36] K.M. Roth, N. Dontha, R.B. Dabke, D.T. Gryko, C. Clausen, J.S. Lindsey, D.F. Bocian, W.G. Kuhr, J. Vac. Sci. Technol. B: Microelectron. Nano. Struct. 18 (2000) 2359.
[37] K.M. Roth, A.A. Yasseri, Z.M. Liu, R.B. Dabke, V. Malinovskii, K.H. Schweikart, L.H. Yu, H. Tiznado, F. Zaera, J.S. Lindsey, W.G. Kuhr, D.F. Bocian, J. Am. Chem. Soc. 125 (2003) 505.
[38] W.-Y. Wong, G.-L. Lu, K.-H. Choi, Y.-H. Guo, J. Organomet. Chem. 690 (2005) 177.
[39] W.-Y. Wong, K.-Y. Ho, S.-L. Ho, Z. Lin, J. Organomet. Chem. 683 (2003) 341.
[40] N. Tajimi, H. Sano, K. Murase, K.-H. Lee, H. Sugimura, Langmuir 23 (2007) 3193.
[41] E.A. Dalchiele, A. Aurora, G. Bernardini, F. Cattaruzza, P. Pallavicini, R. Zanoni, F. Decker, J. Electroanal. Chem. 579 (2005) 133.
[42] A.G. Marrani, F. Cattaruzza, F. Decker, P. Galloni, R. Zanoni, Superlattices Microstruct. 46 (2009) 40.
[43] A. Fidélis, F. Ozanam, J.-N. Chazalviel, Surf. Sci. 444 (2000) L7.
[44] R. Boukherroub, S. Morin, F. Bensebaa, D.D.M. Wayner, Langmuir 15 (1999) 3831.
[45] H.-Z. Yu, S. Morin, D.D.M. Wayner, P. Allongue, C.H. de Villeneuve, J. Phys. Chem. B 104 (2000) 11157.
[46] P.T. Hurley, E.J. Nemanick, B.S. Brunschwig, N.S. Lewis, J. Am. Chem. Soc. 128 (2006) 9990.
[47] R. Zanoni, M. Cossi, M.F. Iozzi, F. Cattaruzza, E.A. Dalchiele, F. Decker, A.G. Marrani, M. Valori, Superlattices Microstruct. 44 (2008) 542.
[48] M. Cossi, M.F. Iozzi, A.G. Marrani, T. Lavecchia, P. Galloni, R. Zanoni, F. Decker, J. Phys. Chem. B 110 (2006) 22961.
[49] B. Fabre, F. Hauquier, J. Phys. Chem. B 110 (2006) 6848.
[50] F. Hauquier, J. Ghilane, B. Fabre, P. Hapiot, J. Am. Chem. Soc. 130 (2008) 2748.
[51] W.-Y. Wong, C.-K. Wong, G.-L. Lu, J. Organomet. Chem. 671 (2003) 27.
[52] R. Zanoni, A. Aurora, F. Cattaruzza, F. Decker, P. Fastiggi, V. Menichetti, P. Tagliatesta, A.L. Capodilupo, A. Lembo, Mater. Sci. Eng. C 27 (2007) 1351.
[53] A.A. Yasseri, D. Syomin, R.S. Loewe, J.S. Lindsey, F. Zaera, D.F. Bocian, J. Am. Chem. Soc. 126 (2004) 15603.
[54] Z.M. Liu, I. Schmidt, P. Thamyongkit, R.S. Loewe, D. Syomin, J.R. Diers, Q. Zhao, V. Misra, J.S. Lindsey, D.F. Bocian, Chem. Mater. 17 (2005) 3728.
[55] L. Wei, D. Syomin, R.S. Loewe, J.S. Lindsey, F. Zaera, D.F. Bocian, J. Phys. Chem. B 109 (2005) 6323.
[56] J.Y. Jiao, P. Thamyongkit, I. Schmidt, J.S. Lindsey, D.F. Bocian, J. Phys. Chem C 111 (2007) 12693.
[57] K. Huang, F. Duclairoir, T. Pro, J. Buckley, G. Marchand, E. Martinez, J.-C. Marchon, B.D. Salvo, G. Delapierre, F. Vinet, ChemPhysChem 10 (2009) 963.
[58] D.A. Van Galen, M. Majda, Anal. Chem. 60 (1988) 1549.
[59] G.A. Schick, I.C. Schreiman, R.W. Wagner, J.S. Lindsey, D.F. Bocian, J. Am. Chem. Soc. 111 (1989) 1344.
[60] K. Padmaja, L.Y. Wei, J.S. Lindsey, D.F. Bocian, J. Org. Chem. 70 (2005) 7972.
[61] F. Anariba, L. Schmidt, A.Z. Muresan, J.S. Lindsey, D.F. Bocian, Langmuir 24 (2008) 6698.
[62] I. Schmidt, J. Jiao, D.F. Bocian, J.S. Lindsey, J. Nanosci. Nanotechnol. 8 (2008) 4813.
[63] P. Thamyongkit, L. Yu, K. Padmaja, J. Jiao, D.F. Bocian, J.S. Lindsey, J. Org. Chem. 71 (2006) 1156.
[64] K. Padmaja, W.J. Youngblood, L.Y. Wei, D.F. Bocian, J.S. Lindsey, Inorg. Chem. 45 (2006) 5479.
[65] I. Schmidt, J. Jiao, P. Thamyongkit, D.S. Sharada, D.F. Bocian, J.S. Lindsey, J. Org. Chem. 71 (2006) 3033.
[66] J. Jiao, F. Anariba, H. Tiznado, I. Schmidt, J.S. Lindsey, F. Zaera, D.F. Bocian, J. Am. Chem. Soc. 128 (2006) 6965.
[67] S. Ciampi, P.K. Eggers, G. Le Saux, M. James, J.B. Harper, J.J. Gooding, Langmuir 25 (2009) 2530.
[68] A.G. Marrani, E.A. Dalchiele, R. Zanoni, F. Decker, F. Cattaruzza, D. Bonifazi, M. Pratoc, Electrochim. Acta 53 (2008) 3903.
[69] T. Pro, J. Buckley, K. Huang, A. Calborean, M. Gely, G. Delapierre, G. Ghibaudo, F. Duclairoir, J.C. Marchon, E. Jalaguier, P. Maldivi, B. De Salvo, S. Deleonibus, IEEE Trans. Nanotechnol. 8 (2009) 204.
[70] S. Ciampi, G. Le Saux, J.B. Harper, J.J. Gooding, Electroanalysis 20 (2008) 1513.
[71] H. Liu, F. Duclairoir, B. Fleury, L. Dubois, Y. Chenavier, J.C. Marchon, Dalton Trans. (2009) 3793.
[72] A. Aurora, F. Cattaruzza, C. Coluzza, C. Della Volpe, G. Di Santo, A. Flamini, C. Mangano, S. Morpurgo, P. Pallavicini, R. Zanoni, Chem. Eur. J. 13 (2007) 1240.
[73] A. Ustione, A. Cricenti, G.G. Condorelli, A. Motta, S. Di Bella, Phys. Stat. Sol. C 2 (2005) 4093.
[74] S. Di Bella, G.G. Condorelli, A. Motta, A. Ustione, A. Cricenti, Langmuir 22 (2006) 7952.
[75] S. Cordier, F. Dorson, F. Grasset, Y. Molard, B. Fabre, H. Haneda, T. Sasaki, M. Mortier, S. Ababou-Girard, C. Perrin, J. Cluster Sci. 20 (2009) 9.
[76] G.G. Condorelli, A. Motta, I.L. Fragalà, F. Giannazzo, V. Raineri, A. Caneschi, D. Gatteschi, Angew. Chem. Int. Ed. 43 (2004) 4081.
[77] G.G. Condorelli, A. Motta, M. Favazza, P. Nativo, I.L. Fragala, D. Gatteschi, Chem. Eur. J. 12 (2006) 3558.
[78] B. Fleury, L. Catala, V. Huc, C. David, W.Z. Zhong, P. Jegou, L. Baraton, S. Palacin, P.-A. Albouy, T. Mallah, Chem. Commun. (2005) 2020.
[79] B. Fleury, V. Huc, L. Catala, P. Jegou, L. Baraton, C. David, S. Palacin, T. Mallah, CrystEngComm 11 (2009) 2192.
[80] G. Pellegrino, A. Motta, A. Cornia, I. Spitaleri, I.L. Fragala, G.G. Condorelli, Polyhedron 28 (2009) 1758.
[81] G.G. Condorelli, A. Motta, G. Pellegrino, A. Cornia, L. Gorini, L.L. Fragala, C. Sangregorio, L. Sorace, Chem. Mater. 20 (2008) 2405.
[82] B. Fleury, F. Volatron, L. Catala, D. Brinzei, E. Rivire, V. Huc, C. David, F. Miserque, G. Rogez, L. Baraton, S. Palacin, T. Mallah, Inorg. Chem. 47 (2008) 1898.
[83] S. Tricard, B. Fleury, F. Volatron, C. Costa-Coquelard, S. Mazerat, V. Huc, C. David, F. Brisset, F. Miserque, P. Jegou, S. Palacin, T. Mallah, Chem. Commun. 46 (2010) 4327.
[84] N. Joo, S. Renaudineau, G. Delapierre, G. Bidan, L.-M. Chamoreau, R. Thouvenot, P. Gouzerh, A. Proust, Chem. Eur. J. 16 (2010) 5043.
[85] N. Gauthier, G. Argouarch, F. Paul, M.G. Humphrey, L. Toupet, S. Ababou-Girard, H. Sabbah, P. Hapiot, B. Fabre, Adv. Mater. 20 (2008) 1952.
[86] M.P. Doyle, W.J. Bryker, J. Org. Chem. 44 (1979) 1572.
[87] J. Pinson, F. Podvorica, Chem. Soc. Rev. 34 (2005) 429.
[88] A. Adenier, M.C. Bernard, M.M. Chehimi, E. Cabet-Deliry, B. Desbat, O. Fagebaume, J. Pinson, F. Podvorica, J. Am. Chem. Soc. 123 (2001) 4541.
[89] A. Adenier, E. Cabet-Deliry, T. Lalot, J. Pinson, F. Podvorica, Chem. Mater. 14 (2002) 4576.
[90] K. Boukerma, M.M. Chehimi, J. Pinson, C. Blomfield, Langmuir 19 (2003) 6333.
[91] P. Allongue, C.H. de Villeneuve, G. Cherouvrier, R. Cortès, M.-C. Bernard, J. Electroanal. Chem. 550–551 (2003) 161.
[92] P. Allongue, C.H. de Villeneuve, J. Pinson, F. Ozanam, J.N. Chazalviel, X. Wallart, Electrochim. Acta 43 (1998) 2791.
[93] M.P. Stewart, F. Maya, D.V. Kosynkin, S.M. Dirk, J.J. Stapleton, C.L. McGuiness, D.L. Allara, J.M. Tour, J. Am. Chem. Soc. 126 (2003) 370.
[94] C.H. de Villeneuve, J. Pinson, M.C. Bernard, P. Allongue, J. Phys. Chem. B 101 (1997) 2415.
[95] B. Chen, A.K. Flatt, H. Jian, J.L. Hudson, J.M. Tour, Chem. Mater. 17 (2005) 4832.
[96] B. Chen, M. Lu, A.K. Flatt, F. Maya, J.M. Tour, Chem. Mater. 20 (2008) 61.
[97] M. Lu, B. Chen, T. He, Y. Li, J.M. Tour, Chem. Mater. 19 (2007) 4447.
[98] M. Lu, T. He, J.M. Tour, Chem. Mater. 20 (2008) 7352.
[99] Z.-H. Peng, Angew. Chem. Int. Ed. 43 (2004) 930.
[100] M. Lu, W.M. Nolte, T. He, D.A. Corley, J.M. Tour, Chem. Mater. 21 (2009) 442.
[101] Q.L. Li, G. Mathur, M. Homsi, S. Surthi, V. Misra, V. Malinovskii, K.H. Schweikart, L.H. Yu, J.S. Lindsey, Z.M. Liu, R.B. Dabke, A. Yasseri, D.F. Bocian, W.G. Kuhr, Appl. Phys. Lett. 81 (2002) 1494.
[102] A. Balakumar, A.B. Lysenko, C. Carcel, V.L. Malinovskii, D.T. Gryko, K.H. Schweikart, R.S. Loewe, A.A. Yasseri, Z.M. Liu, D.F. Bocian, J.S. Lindsey, J. Org. Chem. 69 (2004) 1435.
[103] Q. Zhao, Y. Luo, S. Surthi, Q.L. Li, G. Mathur, S. Gowda, P.R. Larson, M.B. Johnson, V. Misra, Nanotechnology 16 (2005) 257.
[104] W.F. Bergerson, J.A. Mulder, R.P. Hsung, X.-Y. Zhu, J. Am. Chem. Soc. 121 (1998) 454.
[105] H. Qi, S. Sharma, Z. Li, G.L. Snider, A.O. Orlov, C.S. Lent, T.P. Fehlner, J. Am. Chem. Soc. 125 (2003) 15250.
[106] H. Qi, A. Gupta, B.C. Noll, G.L. Snider, Y. Lu, C. Lent, T.P. Fehlner, J. Am. Chem. Soc. 127 (2005) 15218.
[107] P. Nalla, S.H. Huang, Y.B. Zhang, O. Chyan, M.G. Richmond, M. El Bouanani, Chem. Mater. 17 (2005) 5951.
[108] J.C.F. Rodríguez-Reyes, A.V. Teplyakov, Chem. Eur. J. 13 (2007) 9164.
[109] D.A. Skoog, F.J. Holler, T.A. Nieman, Principles of Instrumental Analysis, Harcourt Brace & Co., Orlando, 1998.
[110] R.J. Hamers, Ann. Rev. Anal. Chem. 1 (2008) 707.
[111] A.A. Yasseri, D. Syomin, V.L. Malinovskii, R.S. Loewe, J.S. Lindsey, F. Zaera, D.F. Bocian, J. Am. Chem. Soc. 126 (2004) 11944.
[112] G.C. Herdt, D.R. Jung, A.W. Czanderna, Prog. Surf. Sci. 50 (1995) 103.
[113] R. Zanoni, A. Aurora, F. Cattaruzza, C. Coluzza, E.A. Dalchiele, F. Decker, G. Di Santo, A. Flamini, L. Funari, A.G. Marrani, Mater. Sci. Eng. C 26 (2006) 840.
[114] D. Briggs, M.P. Seah, Practical Surface Analysis, Wiley, Chichester, 1990.
[115] F. Karadas, G. Ertas, S. Suzer, J. Phys. Chem. B 108 (2003) 1515.
[116] J.E. Hutchison, T.A. Postlethwaite, R.W. Murray, Langmuir 9 (1993) 3277.
[117] G.G. Condorelli, A. Motta, C. Bedoya, A. Di Mauro, G. Pellegrino, E. Smecca, Inorg. Chim. Acta 360 (2007) 170.
[118] J.P. Macquet, M.M. Millard, T. Theophanides, J. Am. Chem. Soc. 100 (1978) 4741.
[119] Y. Niwa, H. Kobayashi, T. Tsuchiya, J. Chem. Phys. 60 (1974) 799.
[120] Y. Niwa, H. Kobayashi, T. Tsuchiya, Inorg. Chem. 13 (1974) 2891.
[121] D. Karweik, N. Winograd, D.G. Davis, K.M. Kadish, J. Am. Chem. Soc. 96 (1974) 591.
[122] P.G. Gassman, A. Ghosh, J. Almlof, J. Am. Chem. Soc. 114 (1992) 9990.
[123] K. Tatsumi, M. Tsutsui, J. Am. Chem. Soc. 102 (1980) 882.
[124] J.M. Gottfried, K. Flechtner, A. Kretschmann, T. Lukasczyk, H.-P. Steinruck, J. Am. Chem. Soc. 128 (2006) 5644.
[125] H. Chen, A. Nambu, Wen, J. Graciani, Zhong, J.C. Hanson, E. Fujita, J.A. Rodriguez, J. Phys. Chem. C 111 (2006) 1366.
[126] F. Decker, F. Cattaruzza, C. Coluzza, A. Flamini, A.G. Marrani, R. Zanoni, E.A. Dalchiele, J. Phys. Chem. B 110 (2006) 7374.

[127] F. Anariba, H. Tiznado, J.R. Diers, I. Schmidt, A.Z. Muresan, J.S. Lindsey, F. Zaera, D.F. Bocian, J. Phys. Chem. C 112 (2008) 9474.
[128] M.S. Boeckl, A.L. Bramblett, K.D. Hauch, T. Sasaki, B.D. Ratner, J.W. Rogers, Langmuir 16 (2000) 5644.
[129] M.P. Seah, S.J. Spencer, Surf. Interf. Anal. 35 (2003) 515.
[130] M. Olivier, N. Rochat, A. Chabli, G. Lefeuvre, F. Conne, Mater. Sci. Semicond. Proc. 4 (2001) 15.
[131] Q.L. Li, G. Mathur, S. Gowda, S. Surthi, Q. Zhao, L.H. Yu, J.S. Lindsey, D.F. Bocian, V. Misra, Adv. Mater. 16 (2004) 133.
[132] A.J. Bard, L.R. Faulkner, Electrochemical Methods: Fundamentals and Applications, Wiley, New York, 2001.
[133] E. Laviron, J. Electroanal. Chem. 101 (1979) 19.
[134] S.E. Creager, T.T. Wooster, Anal. Chem. 70 (1998) 4257.
[135] D. Zigah, C. Herrier, L. Scheres, M. Giesbers, B. Fabre, P. Hapiot, H. Zuilhof, Angew. Chem. Int. Ed. 49 (2010) 3157.
[136] R.J. Forster, L.R. Faulkner, J. Am. Chem. Soc. 116 (1994) 5444.
[137] T. He, H. Ding, N. Peor, M. Lu, D.A. Corley, B. Chen, Y. Ofir, Y. Gao, S. Yitzchaik, J.M. Tour, J. Am. Chem. Soc. 130 (2008) 1699.
[138] B. Fabre, S. Cordier, Y. Molard, C. Perrin, S. Ababou-Girard, C. Godet, J. Phys. Chem. C 113 (2009) 17437.
[139] T.A. Keeler, Z. Salman, K.H. Chow, B. Heinrich, M.D. Hossain, B. Kardasz, R.F. Kiefl, S.R. Kreitzman, W.A. MacFarlane, O. Mosendz, T.J. Parolin, D. Wang, Physica B 374–375 (2006) 79.
[140] Z. Salman, A.I. Mansour, K.H. Chow, M. Beaudoin, I. Fan, J. Jung, T.A. Keeler, R.F. Kiefl, C.D.P. Levy, R.C. Ma, G.D. Morris, T.J. Parolin, D. Wang, W.A. MacFarlane, Phys. Rev. B 75 (2007), Art. 073405.
[141] Z. Salman, R.F. Kiefl, K.H. Chow, M.D. Hossain, T.A. Keeler, S.R. Kreitzman, C.D.P. Levy, R.I. Miller, T.J. Parolin, M.R. Pearson, H. Saadaoui, J.D. Schultz, M. Smadella, D. Wang, W.A. MacFarlane, Phys. Rev. Lett. 96 (2006), Art. 147601.
[142] G.D. Morris, W.A. MacFarlane, K.H. Chow, Z. Salman, D.J. Arseneau, S. Daviel, A. Hatakeyama, S.R. Kreitzman, C.D.P. Levy, R. Poutissou, R.H. Heffner, J.E. Elenewski, L.H. Greene, R.F. Kiefl, Phys. Rev. Lett. 93 (2004), Art. 157601.
[143] T.J. Parolin, Z. Salman, J. Chakhalian, Q. Song, K.H. Chow, M.D. Hossain, T.A. Keeler, R.F. Kiefl, S.R. Kreitzman, C.D.P. Levy, R.I. Miller, G.D. Morris, M.R. Pearson, H. Saadaoui, D. Wang, W.A. MacFarlane, Phys. Rev. Lett. 98 (2007), Art. 047601.
[144] J.C. Lin, J.H. Kim, J.A. Kellar, M.C. Hersam, S.T. Nguyen, M.J. Bedzyk, Langmuir 26 (2010) 3771.
[145] D. Gatteschi, R. Sessoli, Angew. Chem. Int. Ed. 42 (2003) 268.
[146] D. Gatteschi, A. Cornia, M. Mannini, R. Sessoli, Inorg. Chem. 48 (2009) 3408.
[147] G.Y. Liu, S. Xu, Y.L. Qian, Acc. Chem. Res. 33 (2000) 457.
[148] R.K. Smith, P.A. Lewis, P.S. Weiss, Prog. Surf. Sci. 75 (2004) 1.
[149] S. Lodha, D.B. Janes, Appl. Phys. Lett. 85 (2004) 2809.
[150] A. Salomon, D. Cahen, S. Lindsay, J. Tomfohr, V.B. Engelkes, C.D. Frisbie, Adv. Mater. 15 (2003) 1881.